MONTE CARLO SOLUTION OF A RADIATIVE HEAT TRANSFER PROBLEM IN A 3-D RECTANGULAR ENCLOSURE CONTAINING ABSORBING, EMITTING, AND ANISOTROPICALLY SCATTERING MEDIUM

A THESIS SUBMITTED TO
THE GRADUATE SCHOOL OF NATURAL AND APPLIED SCIENCES
OF
THE MIDDLE EAST TECHNICAL UNIVERSITY

BY

GÖKMEN DEMİRKAYA

IN PARTIAL FULFILLMENT OF THE REQUIREMENTS FOR THE DEGREE
OF
MASTER OF SCIENCE
IN
THE DEPARTMENT OF MECHANICAL ENGINEERING

DECEMBER 2003

Approval of the Graduate School of Natural and Applied Science

Prof. Dr. Canan Özgen

Director

I certify that this thesis satisfies all the requirements as a thesis for the degree of Master of Science

Prof. Dr. Kemal İder

Head of Department

This is to certify that we have read this thesis and that in our opinion it is fully adequate, in scope and quality, as a thesis for the degree of Master of Science.

Prof. Faruk Arınç

Supervisor

Examining Committee Members

Prof. Dr. Ediz Paykoç (Chairperson)

Prof. Dr. Faruk Arınç (Supervisor)

Prof. Dr. Nevin Selçuk

Asst. Prof. Dr. İlker Tarı

Prof. Dr. Zafer Dursunkaya

ABSTRACT

MONTE CARLO SOLUTION OF A RADIATIVE HEAT TRANSFER PROBLEM IN A 3-D RECTANGULAR ENCLOSURE CONTAINING ABSORBING, EMITTING, AND ANISOTROPICALLY SCATTERING MEDIUM

Demirkaya, Gökmen
M.Sc., Deparment of Mechanical Engineering
Supervisor: Prof. Dr. Faruk Arınç

December 2003, 87 pages

In this study, the application of a Monte Carlo method (MCM) for radiative heat transfer in three-dimensional rectangular enclosures was investigated. The study covers the development of the method from simple surface exchange problems to enclosure problems containing absorbing, emitting and isotropically/anisotropically scattering medium.

The accuracy of the MCM was first evaluated by applying the method to cubical enclosure problems. The first one of the cubical enclosure problems was prediction of radiative heat flux vector in a cubical enclosure containing purely, isotropically and anisotropically scattering medium with non-symmetric boundary conditions. Then, the prediction of radiative heat flux vector in an enclosure containing absorbing, emitting, isotropically and anisotropically scattering medium with symmetric boundary conditions was evaluated. The predicted solutions were compared with the solutions of method of lines solution (MOL) of discrete ordinates method (DOM).

The method was then applied to predict the incident heat fluxes on the freeboard walls of a bubbling fluidized bed combustor, and the solutions were compared with those of MOL of DOM and experimental measurements.

Comparisons show that MCM provides accurate and computationally efficient solutions for modelling of radiative heat transfer in 3-D rectangular enclosures containing absorbing, emitting and scattering media with isotropic and anisotropic scattering properties.

Keywords: Monte Carlo Method, Radiative Heat Transfer, Scattering Medium

ÖZ

EMEN, IŞIYAN, VE İZOTROPİK-OLMAYAN SAÇINIM YAPAN ORTAM
İÇEREN ÜÇ BOYUTLU DİKDÖRTGEN HACİMLERDE
IŞINIM ISI TRANSFER PROBLEMİNİN
MONTE CARLO ÇÖZÜMÜ

Demirkaya, Gökmen
Yüksek Lisans, Makina Mühendisliği Bölümü
Tez Yöneticisi: Prof. Dr. Faruk Arınç

Aralık 2003, 87 sayfa

Bu çalışmada, üç boyutlu dikdörtgen hacimlerde Monte Carlo metodunun (MCM) ışınım ısı transferine uygulanması araştırıldı. Bu çalışma, metodun basit yüzey değişim problemlerinden emen, ışıyan, ve izotropik/izotropik olmayan saçınım yapan ortam içeren hacim problemlerine geliştirilmesini kapsamaktadır.

MCM'nin doğruluğu ilk olarak kübik hacimli problemlerde uygulanarak geliştirildi. Kubik hacimli problemlerden birincisi, ışınım ısı akısının simetrik olmayan sınır koşullarına sahip, saf izotropik ve izotropik olmayan saçınım yapan ortam içeren kubik hacimde tahmin edilmesidir. Sonra, ışınım ısı akısı doğrultusunun emen, yayan, izotropik ve izotropik olmayan saçınım yapan ortam içeren hacimde tahmini gerçekleştirildi. Tahmin edilen sonuçlar, belirli yönler yönteminin çizgiler metoduyla çözümünden elde edilen sonuçlarla karşılaştırıldı.

Metod daha sonra atmosferik, kabarcıklı, akışkan yataklı bir yakıcının serbest bölgesine düşen ısı akısını tahmin etmek için uygulanmış ve sonuçları belirli yönler yönteminin çizgiler metodu ve deneysel ölçüm sonuçlarıyla karşılaştırıldı.

Karşılaştırmalar, ışınım ısı transferinin emen, yayan, izotropik ve izotropik olmayan özelliklere sahip saçınım yapan ortam içeren üç boyutlu, dikdörtgenler prizması biçimindeki hacimlerde modellenmesi için MCM'nin, doğru ve bilgisayar zamanı açısından ekonomik çözümler verdiğini göstermiştir.

Anahtar Kelimeler: Monte Carlo metodu, Işınım Isı Transferi, Saçınım Yapan Ortam

ACKNOWLEDGEMENTS

The author wishes to express sincere appreciation to Prof. Dr. Faruk Arınç for his guidance and insight throughout the research.

In addition, I would like to thank Prof. Dr. Nevin Selçuk for her guidance, contributions and encouragement.

I must say a special thank you to faculty member Asst. Prof. İlker Tarı for his suggestions and comments. I am most grateful to Hakan Ertürk and Işıl Ayrancı whose theses were a guide and for their help throughout the study.

The author also wishes to express his deepest thanks to his family, Adem-Hatice-Nazlı Demirkaya for their support, patience and encouragement. Special thanks are owed to my big brother Gökhan for his support and motivation during the whole study.

I wish to extend my thanks to Balkan, Orhan and Serkan for their suggestions, ideas and encouragement.

Finally, my ex-home mates Murat, Yılmaz and existing home mate Bora's contributions to my study are also highly appreciated.

TABLE OF CONTENTS

LIST OF TABLES

TABLES

LIST OF FIGURES

FIGURES

LIST OF SYMBOLS

A	:	Area (m^2)
E	:	Emissive power (W/m^2), Percentage error
$\hat{e}_1, \hat{e}_2$	:	Unit vectors indicating local x and y direction
F_{ij}	:	View factor of surface i to surface j
H	:	Height of enclosure (m)
h	:	Planck's constant ($=6.6262 \times 10^{-34}$ J.s)
I	:	Radiation intensity ($W/m^2 sr$)
$\hat{i}, \hat{j}, \hat{k}$	:	Unit vectors in x,y and z directions
k	:	Boltzmann's constant (=1.3806 J/K)
L	:	Length of the enclosure (m)
L_x, L_y, L_z	:	Dimensions in x,y and z directions (m)
L_w	:	Distance photon bundle will travel before being absorbed by wall (m)
L_κ	:	Distance photon bundle will travel before being absorbed by medium (m)
L_σ	:	Distance photon bundle will travel before being scattered by medium (m)
nh	:	Number of history
$\hat{n}$	:	Unit normal vector
P	:	Probability function
q	:	Net radiative exchange, radiative flux density (W/m^2)
Q	:	Heat transfer rate (W)
Q_{ext}	:	Extinction efficiency
Q_{sca}	:	Scattering efficiency
r	:	Position vector (m)

R	:	Random number
$\hat{s}$	:	Direction unit vector of photon bundle
S	:	Distance between points on enclosure surface (m)
t	:	Time (s)
T	:	Absolute temperature (K)
$\hat{t}_1, \hat{t}_2$	:	Unit tangent vector
V	:	Volume (m^3)
W	:	Width of the enclosure (m)
w	:	Energy per photon bundle (W)
x, y, z	:	Cartesian coordinates (m)

Greek Symbols

α	:	Absorptivity, angle between $\hat{t}_1$ and $\hat{t}_2$
β	:	Extinction coefficient (m^{-1})
δ	:	Line spacing (m^{-1})
ε	:	Emissivity
$\Phi(\hat{s}\cdot\hat{s}')$	:	Scattering phase function
η	:	Wave number (m^{-1})
κ	:	Absorption coefficient (m^{-1})
λ	:	Wavelength (μm)
θ	:	Polar angle (rad)
σ	:	Stefan-Boltzmann constant ($=5.67 \times 10^{-8}$ W/m^2K^4)
	:	Scattering coefficient (m^{-1})
τ	:	Optical thickness
ψ	:	Azimuthal angle (rad)
ω	:	Single scattering albedo
Ω	:	Solid angle (sr)

Subscripts

a	:	Absorbing
b	:	Blackbody

bottom	:	Bottom
e	:	Emission
exact	:	Exact value
predicted	:	Predicted value
G, g	:	Gas
i	:	Incident, incoming
max	:	Maximum
min	:	Minimum
n	:	In normal direction
o	:	Initial, reference value, outgoing
p	:	Particle
r	:	Reflected
top	:	Top
w	:	Wall
x, y, z	:	In a given direction
θ, ψ	:	In a given direction
λ	:	At a given wavelength
η	:	At a given wavenumber
∞	:	Infinity

Superscripts

^	:	Vector
*	:	Dimensionless

Abbreviations

ABFBC	:	Atmospheric bubbling fluidized bed combustor
CPU	:	Computer processing unit
DOM	:	Discrete ordinates method
MOL	:	Method of lines
MCM	:	Monte Carlo method
RTE	:	Radiative transfer equation

CHAPTER 1

INTRODUCTION

The analysis of radiative heat transfer has been an important field in heat transfer research over the past 40 years because of its necessity in high temperature applications such as rocket nozzles, space shuttles, engines, and the like. Thermal radiation is a significant mode of heat transfer in many modern engineering applications. Some specific areas include the design and analysis of energy conversion systems such as furnaces, combustors, solar energy conversion devices, and the engines where high temperatures are present to ensure the thermodynamic efficiency of the processes, and where other modes of heat transfer may also be significant.

The researchers have focused on the invention of new technologies from the start of 1950's. The world has faced with environmental problems starting from 1970's due to inefficient use of fuels and combustion systems. This has directed the researchers to focus on increasing the overall thermal efficiencies and modifications of furnaces. In this mean time, mathematical models that simulate the combustion in furnaces have become important because of their low cost as compared with experiments. The fast developments in the computer technology in the last three decades have helped mathematical modeling to become a popular method in predicting the complete combustion behavior of furnaces.

A combination of a turbulence model, a heat transfer model, and a chemical model forms a complete combustion model. Heat transfer in most combusting flows is strongly affected by radiative exchanges. The dominant mechanism of heat transfer at high temperatures in most furnaces and combustors is thermal radiation. A realistic mathematical modeling of radiation should be used for the complete combustion model. Its modeling is a rather difficult task because of long range interaction and spectral and directional variation of radiative properties.

In many engineering applications, the interaction of thermal radiation with radiatively participating medium exists. Participating medium must be accounted for in the mathematical modeling of radiative heat transfer, especially in burning of any fuel. Furnaces or combustion chambers can be modeled as enclosures containing a radiatively absorbing, emitting, and scattering medium. The chemical reaction of fuel generates the combustion products which form the participating medium exchanging heat with the enclosure surfaces.

The equation of radiative transfer, which describes the radiative intensity field within the enclosure as a function of location, direction, and spectral variable, is an integro-differential equation containing highly non-linear terms. In order to obtain the net radiation heat flux crossing a surface element, the contributions of radiative energy irradiating the surface from all possible directions and spectra must be summed up. After considering energy balance in an infinitesimal volume, integration of equation of radiative heat transfer over all directions and wavelength spectrum should be made. In most of the problems, it is impossible to handle these integrals by analytical means especially when the radiative properties are functions of location, direction and spectral variable at a given time. Obviously, a complete solution of this equation is truly a formidable task.

Approximate solution methods are used when the radiative properties are functions of location, direction, and spectral variable at a given time. Accuracy, simplicity, and the computation effort are the important parameters for approximate solution methods.

A survey of the literature over the past several years demonstrates that some solution methods have been used frequently. The Monte Carlo method is one of the methods used frequently in radiation problems which is based on the physical nature of thermal radiation by direct simulation of photon bundles. This method has been found to be more readily adaptable to more difficult situations than others. The integral that governs the emission of radiant energy depends on various parameters such as wave length, angle of emission, and the nature of the medium. Also, different integrals govern the reflection and scattering processes. Radiation problems possess a form ideally suited for Monte Carlo application, since it provides a vehicle to numerically evaluate multiple integrals.

The outcome of combustion models depends on the accuracy of the radiation algorithm. Although the Monte Carlo method can provide good results for radiation problems, sometimes different results are obtained for the same problem among different researchers mostly due to the use of different random number generators and/or algorithms such as variance reduction. Therefore, in this study, the accuracy of Monte Carlo method is re-examined by applying it to several three-dimensional radiative heat transfer problems with participating media and comparing its predictions with MOL of DOM solutions.

The predictive accuracy of the method was examined for (1) a cubical enclosure problems containing purely scattering and absorbing, emitting scattering medium with isotropic and anisotropic scattering properties by validating the solutions against MOL of DOM solutions available in the literature; and (2) a physical problem which is the freeboard of pilot-scale atmospheric, bubbling fluidized bed combustor by comparing its predictions with those of the MOL of DOM and measurements.

CHAPTER 2

LITERATURE SURVEY

The literature survey on Monte Carlo method is presented in two parts of this chapter. First, radiative heat transfer applications of the method and the literature on similar problems handled in this study are presented. Then, problems selected for this study are introduced in the last part.

2.1 APPLICATIONS, DEVELOPMENTS AND MODIFICATIONS OF MONTE CARLO METHODS

John Howell and his coworker Perlmutter [1] first applied Monte Carlo methods to problems of radiative heat transfer in participating medium. They initially solved the radiation through grey gases between infinite parallel planes. The local gas emissive power and the net energy transfer between the plates were calculated. Two cases were examined, the first case being a gas with no internal energy generation contained between plates at different temperatures, and the second case being a gas with uniformly distributed energy sources between plates at equal temperatures. Analytical solution of Usiskin and Sparrow [2] and modified diffusion approximation solution of Deissler [3] were utilized as bases for checking the accuracy of the obtained Monte Carlo method solutions. They concluded that Monte Carlo method could be easily adapted and applied to gas radiation problems.

After the first study, Howell and Perlmutter [4] continued with a more difficult problem than infinite parallel plates. It was determination of the emissive power distribution and local energy flux in a grey gas within an annulus between concentric cylinders. Because of the analytical difficulties of this case, no exact result was available. They compared the Monte Carlo results with Deissler [3] diffusion approximation results, and found out that the results were in good agreement.

Following with similar applications, Howell [5] reviewed the applications of the method in heat transfer problems including radiative transfer problems based on his experience in the area. He concluded that Monte Carlo methods had a definite advantage over other radiative transfer calculation techniques when the difficulty of the problem lied above some undefined level, and that complex problems could be treated by Monte Carlo method with greater flexibility, simplicity, and speed.

In recent years, Haji-Sheikh [6] has developed modifications of the Monte Carlo method. He applied the Monte Carlo method to radiation, conduction, and convection problems. He made modifications on the Monte Carlo method by introducing "importance sampling" in the algorithms. Initially, Howell and Perlmutter [1, 4] popularized the idea of biasing photon bundles toward the spectral and angular regions with higher emitted radiant energy. When the surface properties exhibit strong dependence on the wavelength within narrow bands, the unbiased method permits only a small fraction of energy bundles to have wavelengths within these narrow bands. This causes an inefficient use of computer time. In order to eliminate this undesirable situation, the selection of energy bundles may be biased towards wavelengths at which the radiant energy is significant.

Another study carried out by Mochida *et al*. [7], aimed to develop a method to numerically analyze transient characteristics of combined radiative and conductive heat transfer in vacuum furnaces heated by radiant tube burners. For this purpose, in radiative heat exchange calculations, a Monte Carlo method was preferred. The results of the numerical simulations were compared with the results of the experiments. The comparison indicated that the simulated results agreed very well with the experimental ones.

Taniguchi *et al.* [8] applied Monte Carlo method to the development of a simulation technique for radiation-convection heat transfer in the high temperature fields of industrial furnaces, boilers, and gas turbine combustors. Convection and radiation effects require different equations to analyze and therefore arranging both of these effects using the same type of equation is quite difficult. While the convection effect necessitates a differential equation, radiation effect and integral equation needs to be analyzed. Thus, in order to overtake this difficulty, the researchers introduced the zone method and Monte Carlo method for the integral equation of the radiation effect, and the finite difference method for the differential equation of the convection effect.

This developed technique on combined heat transfer phenomena of radiation and convection was tested by two analytical examples, which were the high temperature field of an industrial furnace and the ambient temperature field of a living room.

Although there are many recent studies performed on the radiative transfer in a medium with variable spatial refractive index, none of these works have taken scattering into account. Liu *et al*. [9] developed a Monte Carlo curved ray-tracing method to analyze the radiative transfer in one-dimensional, absorbing, emitting, scattering, semi-transparent slab with variable spatial refractive index. Moreover, a problem of radiative equilibrium with linear variable spatial refractive index was taken as an example.

In literature, due to its good ability to treat complex boundary geometry and anisotropic scattering, Monte Carlo method is often preferred to simulate the radiative transfer in media with uniform refractive indices. However, the main problem with Monte Carlo simulation is the ray tracing. Liu et al. [9] used the curved ray tracing technique developed by Ben Abdallah and coworkers [10].

In the light of the results of their study, it is concluded that Monte Carlo curved ray tracing method has a good accuracy in solving the radiative transfer in one-dimensional, semi-transparent slab with variable spatial refractive index. Furthermore, it was found that the influences of refractive index gradient were important and the influences increased with the refractive index gradient. Consequently, the results demonstrated the similarity of the effect of scattering phase function to that in the medium with constant refractive index.

In another study of L. H. Liu and his co-worker [11], Monte Carlo ray tracing method (MCRT) based on the concept of radiation distribution factor was extended to solve a radiative heat transfer problem in turbulent fluctuating medium under the optically thin fluctuation approximation. This study examined a one-dimensional, non-scattering turbulent fluctuating medium and solved the distribution of the time-averaged volume radiation heat source by two methods, MCRT and direct integration method. Comparison of the methods shows that the results of MCRT based on concept of radiation distribution factor agree with the results of integration solution very well. However, the results obtained from MCRT based on concept of radiative transfer coefficient were not in agreement with the result of integration solution.

A vector Monte Carlo method is developed to model the transfer of polarized radiation in optically thick, multiple scattering, particle-laden semi-transparent medium by Mengüç *et al*. [12]. They introduced the description of the theoretical background of the method and validated against references of a plane-parallel geometry available in the literature. After applying the Monte Carlo method, in the case of a purely scattering medium, the results are validated in good agreement and they concluded that the new Vector Monte Carlo method can be applied to radiation problems.

Coquard *et al*. [13] characterized the radiative properties of beds of semi-transparent spherical particles by Monte Carlo method. The analysis of radiative behavior of the bed was performed by ray-tracing simulation and computation of the radiative property of a homogenous semi-transparent medium. They summarized that characterization of evolution of the radiative properties of the bed was reasonably good by Monte Carlo method. Also, they emphasized that this method permitted to delimit the range of validity of the independent scattering hypothesis.

Monte Carlo method for thermal radiation was applied to buoyant turbulent diffusion combustion models by Snergiev [14]. He optimized the photon bundles to the spatial distribution of radiative emissive power. The results were good with an acceptable computational cost.

Wong and Mengüç [15] used Monte Carlo method to solve the Boltzmann transport equation, which is the governing equation for radiative transfer. They used different photon bundle profiles for a highly scattering medium. For different profiles, they found out that radial distribution of photons affected the solutions.

Yu *et al*. [16] worked on determination of characteristics of a semi-transparent medium containing small particles by Monte Carlo method. The scattering characteristic of an isotropic medium has wide application areas such as power engineering, optical science and biotechnology. Monte Carlo method was used to predict the radiative characteristics of a semi-transparent medium containing small particles. They studied radiation in a semi-transparent planar slab. During their study, they found that the results were dependent on path length methods. The proper choice of path length method gave better results for particle anisotropic scattering.

The presence of coal particles significantly affects the solution of radiative transfer solutions in coal-fired furnaces. Therefore, absorbing, emitting and scattering of particles are expected to be a key parameter for radiative heat transfer problems. Marakis *et al*. [17] investigated the particle influence on radiation. They found out that the physical realistic approach for the scattering behavior of coal combustion particles was anisotropic, strongly forward scattering. Moreover, they advised that instead of using scattering algorithm, neglecting of the scattering was a reasonable approach in atmospheric coal combustion.

Cai [18] presented a general ray tracing procedure in industrial enclosures of arbitrary geometry containing transparent or participating medium with diffuse or specular surfaces. The generalized exchange factors were calculated, allowing the consideration of specular and semi-transparent surfaces, by a pseudo Monte Carlo method which was a deterministic ray tracing method. He concluded that Monte Carlo could easily treat problems having surfaces with directional emission and high specularity.

Ertürk *et al.* [19, 20] applied Monte Carlo method to several test problems with three-dimensional geometries for evaluating the accuracy of the Monte Carlo method. The first problem was an idealized enclosure problem, which had analytical solutions evaluated by Selçuk [21]. The idealized situation considered was a cubical enclosure with black interior walls, containing grey, non-scattering medium of an optical thickness of unity which was in thermal equilibrium with its bounding walls. He concluded that the solution efficiency was highly dependent on the ray tracing procedure, the form of representation of energy in terms of photon bundles, the grid size, and the total number of photon histories utilized. He also checked two different ray-tracing algorithms on the optically thin medium. He emphasized that utilizing discrete photon bundles rather than partitioning the energy of the bundle through the path length traveled, was more efficient.

The second problem investigated by Ertürk *et al* [19, 20] was a box-shaped enclosure problem for which Selçuk [22] obtained exact numerical solutions. The enclosure had black interior walls and an absorbing, emitting medium of constant properties. The cases of assigning constant energy per bundle, and assigning energy per bundle based on the emissive power of the sub-regions of emissions were compared. The former case was found to be more efficient than the latter one. It was concluded that increase in grid number did not increase the accuracy for the same total number of photon bundle histories. It was also concluded that the number of photon bundle histories affected accuracy more than the number of sub-regions utilized.

Non-grey treatment of radiative properties results in appearance of an additional variable in radiative transfer equation, i.e., wavelength, which usually made the problem very laborious for most of the numerical solution techniques. However, the most accurate way of modeling radiative behavior in the presence of absorbing, emitting gases like carbon dioxide and water vapor is to consider spectral variation. The third problem investigated by Ertürk *et al* [19, 20] was Tong and Skocypec's [23] three-dimensional problem with isothermal non-grey gas. Monte Carlo method was applied to obtain the solution for a rectangular, cold, and black enclosure containing non-grey, absorbing, emitting and scattering medium. Participating medium was a mixture of carbon particles and nitrogen and carbon dioxide gases. Ertürk *et al* [19, 20] stressed on the importance of integration techniques for spectral integrals. They obtained different predictions, which were different in one or more orders of magnitude with different integration techniques. They also concluded that Monte Carlo method could handle problems of large variety without a great increase in complication of the solution technique and computation labor.

Monte Carlo method is also used for validation purposes of some other solution methods. I. Ayrancı [24] examined the 3-D cubical enclosure problems of Kim and Huh [25]. She used the method of lines solution (MOL) of discrete ordinates method (DOM) to predict heat flux and incident radiation distributions for absorbing, emitting and isotropically/anisotropically scattering medium and compared the results to that of Monte Carlo method.

2.2 PROBLEMS SELECTED FOR THIS STUDY

In this study, the Monte Carlo method was used to predict the radiative heat transfer in several geometries.

The prediction accuracy of the code was first obtained by applying the code to cubical enclosure bounded by black surfaces with participating medium. The solutions were compared with the MOL of DOM solutions available in the literature [24]. Then, the method was used for a 3-D rectangular enclosure with grey/black walls containing absorbing, emitting and isotropically scattering medium. The Monte Carlo predictions were compared against MOL solution of DOM, and experimental measurements [26, and 27].

Selçuk *et al*. [26, and 27] analyzed the radiative heat transfer in the freeboard of the 0.3 MW_t atmospheric bubbling fluidized bed combustor (ABFBC) containing particle-laden combustion gases. In order to apply numerical methods to the freeboard test rig, the temperature and radiative properties of the surfaces and the medium were obtained. In addition, the freeboard section of the combustor was treated as a 3-D rectangular enclosure containing absorbing, emitting and isotropically scattering medium bounded by diffuse, grey/black walls. The radiative properties of the particle-laden combustion gases and the radiative properties and temperatures of the bounding surfaces were given in the references [24, 26, 27, 28, and 29]. Also, polynomials representing the medium and the side-wall temperature profiles were determined. All these data provide the necessary information to model the problem realistically and to apply the Monte Carlo method to the problem.

CHAPTER 3

THE MONTE CARLO METHOD

The Monte Carlo Method, a branch of experimental mathematics, is a method of directly simulating mathematical relations by random processes. As a universal numerical technique, Monte Carlo method could only have emerged with the appearance of computers. The field of application of the method is expanding with each new computer generation.

One advantage of the Monte Carlo method is the simple structure of the computation algorithm. As a rule, a program is written to carry out one random trial. This trial is repeated N times, each trial is being independent of the others, and then the results of all trials are averaged. A second feature of the method is that, as a rule, the error of calculations is proportional to $\sqrt{(D/N)}$, where D is some constant, and N is the number of trials.

In physics, the Monte Carlo method has been used to solve numerous types of diffusion problems. In heat transfer, radiation and conduction have dominated the use of the Monte Carlo method, while its application to convective problems has been insignificant, despite the fact that, for instance, the transport of energy in a turbulent flow depends on random processes. In radiation transfer, it has been extensively employed to solve general radiation heat transfer problems as well as radiative transfer problems in multidimensional enclosures and furnaces.

In the field of heat transfer, problems in thermal radiation are particularly well suited to a solution by the Monte Carlo technique since energy travels in discrete parcels, named as photons. It travels relatively long distances along a straight path before interaction with matter.

The method is based on simulating a finite number of photon bundles that carry finite amount of radiative energy using a random number generator. The physical events such as emission, reflection, absorption, and scattering that happen in the life of a photon bundle are all decided using the probability density functions derived from the physical laws and random numbers. The surfaces or the gas volume which will be modeled, are first divided into a number of sub-regions each of which emitting and absorbing photon bundles accordingly to its temperature, emissivity, absorptivity and transmissivity. Each photon history is started from a sub-region by assigning a set of values to the photon, i.e., initial energy, position, and direction. Following this, mean free path that the photon propagates is determined, stochastically. Then, the absorption and scattering coefficients are sampled, and it is determined whether the collided photon is absorbed or scattered by the gas molecules or particles in the medium. If it is absorbed, the history is terminated. If it is scattered, the distribution of scattering angles is sampled and a new direction is assigned to the photon.

3.1 REPRESENTING ENERGY IN TERMS OF PHOTON BUNDLES

According to the quantum theory, energy is transferred through radiation in terms of energy particles named as photons. Based on this theory, the Monte Carlo method, which is a statistical method, simulates the energy transfer by observing and collecting data about the behavior of a number of photon bundles. The accuracy of the method increases as the number of bundles during the simulation is increased according to the rules of statistics.

In solving thermal radiation problems with Monte Carlo method, the energy of each emitted photon bundle, w, is represented by,

$$w = \frac{E}{nh} \tag{3.1}$$

where E is the total emissive power, nh is the number of histories used for the simulation.

The emissions of the photons are from either surfaces or the medium enclosed by the surfaces. During simulations, in order to obtain localized results, these surfaces and medium must also be divided into some sub-regions, which are area elements for surfaces and volume elements for a gas medium. As shown in Eq. (3.1), while defining the number of photon bundles emitted from a sub-region, the emissive power of the sub-region is used. The emissive power for a surface element, E_{bw}, and for a gas volume, E_{bg}, can be evaluated by using,

$$E_{bw}=\varepsilon\sigma T_w^4 A \tag{3.2}$$

$$E_{bg}=4\kappa\sigma T_g^4 V \tag{3.3}$$

In Eq. (3.2) and (3.3), A is the area, V is the volume, ε is the emissivity of the surface, and κ is the absorption coefficient of the medium.

3.2 SELECTING FROM PROBABILITY DISTRIBUTIONS

There is no single Monte Carlo method; rather, there are different statistical approaches. In its simplest form, the method consists of simulating a finite number of photon histories using a random number generator. During the simulation of a photon history, in order to follow the bundle in statistically meaningful way, all the physical events such as the points and directions of emissions and incidence, and wavelengths of emission, absorption, reflection, and scattering, must be considered according to probability distributions using random numbers. The first step of choosing from a probability distribution is evaluating the random number. In order to evaluate the random number relation, the cumulative distribution function must be obtained.

The general definition for a cumulative distribution function of a physical event P, which is a function of property ξ that occurs between the maximum and minimum values ξ_{max} and ξ_{min}, is given by,

$$\frac{\int_0^{R_\xi} d\xi}{\int_0^1 d\xi} = \frac{\int_{\xi_{min}}^{\xi} P(\xi)d\xi}{\int_{\xi_{min}}^{\xi_{max}} P(\xi)d\xi} \tag{3.4}$$

where R_ξ is a random number which can be defined as a function of ξ and has a value between zero and one.

When the integrals of Eq. (3.4) are evaluated, the resulting cumulative distribution function is in the form,

$$R_\xi = R_\xi(\xi) \tag{3.5}$$

Then, the random number relation, which is given in Eq. (3.6), is obtained by inverting the cumulative distribution function given by Eq. (3.5),

$$\xi = \xi(R_\xi) \tag{3.6}$$

3.3 SURFACE EXCHANGE AND SURFACE EMISSIONS

In most applications, the first step in a Monte Carlo simulation is setting the appropriate geometry for the emissions, ray tracing, and absorption of photon bundles. The surfaces are generally divided into smaller area elements for which the local properties can be utilized to obtain local heat flux values.

The cumulative distribution functions that are used to obtain the random number relations for evaluating points of emissions from surfaces can be obtained by inverting the following equations,

$$R_x = \frac{\int_{x_{min}}^{x} \int_{y_{min}}^{y_{max}} \varepsilon E_{bw}\, dydx}{\int_{x_{min}}^{x_{max}} \int_{y_{min}}^{y_{max}} \varepsilon E_{bw}\, dydx} \tag{3.7}$$

$$R_y = \frac{\int_{y_{min}}^{y} \int_{x_{min}}^{x_{max}} \varepsilon E_{bw}\, dxdy}{\int_{y_{min}}^{y_{max}} \int_{x_{min}}^{x_{max}} \varepsilon E_{bw}\, dxdy} \tag{3.8}$$

where x and y are the variables of the rectangular coordinates.

The random number relations that are used to evaluate points of emissions from the rectangular surface sub-regions of constant temperature and absorption coefficient are given by,

$$x_e = R_x (x_{max} - x_{min}) + x_{min} \tag{3.9}$$

$$y_e = R_y (y_{max} - y_{min}) + y_{min} \tag{3.10}$$

where x_e and y_e are the points of emissions, x_{max}, y_{max}, x_{min}, and y_{min} are the maximum and minimum coordinates of a rectangular area sub-region in terms of rectangular coordinate variables x and y, respectively.

In most of the problems, even if there exist a temperature variation throughout a sub-region, Eq. (3.9) and (3.10) can still be used to represent the sub-region with a mean or center point temperature value.

Three vectors, two of which are unit tangents to the surface, can define a surface in three-dimensional space, and the remaining one is the unit surface normal. The unit surface normal can be represented by,

$$\hat{n} = \frac{\hat{t}_1 \times \hat{t}_2}{\left|\hat{t}_1 \times \hat{t}_2\right|} \tag{3.11}$$

The direction of emission of the emitted bundle can be determined by the polar angle which is the angle between the unit surface normal and the photon bundle, together with the azimuthal angle which is the angle between the projection of the photon bundle on the surface which $\hat{t}_1$ and $\hat{t}_2$ are tangent to, and $\hat{t}_1$. The random number relations for the azimuthal angle, ψ, and the polar angle, θ, are given by the following relations:

$$\psi = 2\pi R_{\psi} \tag{3.12}$$

$$\theta = \arcsin(\sqrt{R_{\theta}}) \tag{3.13}$$

3.4 EMISSIONS FROM PARTICIPATING MEDIUM

Similar to the above cases, the medium can be divided into smaller volume elements so that the local properties can be utilized to evaluate the local values for divergence of radiative flux densities.

The cumulative distribution functions that are used to obtain the random number relations for evaluating points of emissions from the gas medium can be obtained by reversing the following expressions,

$$R_x=\frac{\int_{x_{min}}^{x}\int_{y_{min}}^{y_{max}}\int_{z_{min}}^{z_{max}}\varepsilon E_{bg}dzdydx}{\int_{x_{min}}^{x_{max}}\int_{y_{min}}^{y_{max}}\int_{z_{min}}^{z_{max}}\varepsilon E_{bg}dzdydx} \tag{3.14}$$

$$R_y=\frac{\int_{y_{min}}^{y}\int_{x_{min}}^{x_{max}}\int_{z_{min}}^{z_{max}}\varepsilon E_{bg}dzdxdy}{\int_{y_{min}}^{y_{max}}\int_{x_{min}}^{x_{max}}\int_{z_{min}}^{z_{max}}\varepsilon E_{bg}dzdxdy} \tag{3.15}$$

$$R_z=\frac{\int_{z_{min}}^{z}\int_{x_{min}}^{x_{max}}\int_{y_{min}}^{y_{max}}\varepsilon E_{bg}dydxdz}{\int_{z_{min}}^{z_{max}}\int_{x_{min}}^{x_{max}}\int_{y_{min}}^{y_{max}}\varepsilon E_{bg}dydxdz} \tag{3.16}$$

The random number relations that are used to evaluate points of emissions from rectangular parallel-piped volumetric sub-regions of constant temperature and absorption coefficient can be obtained from,

$$x_e = R_x(x_{max} - x_{min}) + x_{min} \tag{3.17}$$

$$y_e = R_y(y_{max} - y_{min}) + y_{min} \tag{3.18}$$

$$z_e = R_z(z_{max} - z_{min}) + z_{min} \tag{3.19}$$

where x_e, y_e and z_e are the points of emissions, x_{max}, y_{max}, z_{max}, x_{min}, y_{min} and z_{min} are the maximum and minimum coordinates of a parallelepiped volumetric sub-region in terms of rectangular coordinate variables x, y, and z, respectively.

Similar to the surface emissions, the temperature throughout the whole sub-region can be assumed equal to a representative temperature value even if there is a temperature variation within the sub-region.

The points of emission can also be selected from a uniform distribution without generating any random number.

The azimuthal angle of the emitted photon bundle can still be evaluated from Eq. (3.12) while the polar angle shown in Fig. 3.1 can be obtained by using Eq. (3.20). The change in the random number relation for the polar angle is due to the change in integration limits from 0 to π/2 for the surface emissions, and from – π/2 to π/2 for volumetric gas emission,

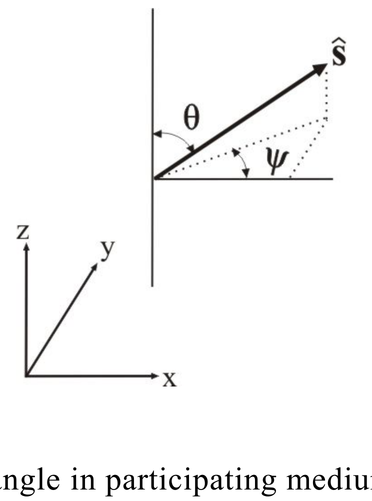

Figure 3-1 The polar angle in participating medium

$$\theta = \arccos(1 - 2R_\theta) \tag{3.20}$$

The evaluation of the wave number with a random number relation is usually more complicated than the evaluation of the preceding random number relation because the spectral variation of the participating medium is defined by more complicated equations than those of points or directions of emission. The cumulative distribution function for the wave number is given by,

$$R_\eta(\eta) = \frac{\int_0^1 \kappa_\eta E_{b\eta} d\eta}{\int_0^\infty \kappa_\eta E_{b\eta} d\eta} \tag{3.21}$$

where κ_η the spectral absorption coefficient, and $E_{b\eta}$ is the spectral blackbody emissive power of the medium.

The cumulative distribution function obtained by Eq. (3.21) can be usually inverted by numerical methods to obtain wave number random relation,

$$\eta = \eta(R_\eta) \tag{3.22}$$

3.5 RAY TRACING

During the simulation, the step following the evaluation of points of emission and wavelength is the evaluation of the direction of the photon bundle by using the random number relations for polar and azimuthal angles.

As shown in Fig. 3-2, the unit direction vector represented by the polar angle θ measured from the surface normal, and the azimuthal angle ψ

measured from $\hat{t}_1$ can be calculated by,

$$\hat{s} = \frac{\sin\theta}{\sin\alpha}\left[\sin(\alpha - \psi)\hat{t}_1 + \sin\psi\hat{t}_2\right] + \cos\theta\hat{n} \tag{3.23}$$

where α is the angle between $\hat{t}_1$ and $\hat{t}_2$. For the rectangular coordinate system, which is the coordinate system used throughout this study, α = π /2, and the Eq. (3.23) reduces to,

$$\hat{s} = \sin\theta\left[\cos\psi\hat{t}_1 + \sin\psi\hat{t}_2\right] + \cos\theta\hat{n} \tag{3.24}$$

The photon bundle can then be traced until it is absorbed by the gas medium or by a surface it collides with. Different ray tracing algorithms simulating the physical events with different statistical approaches can be utilized.

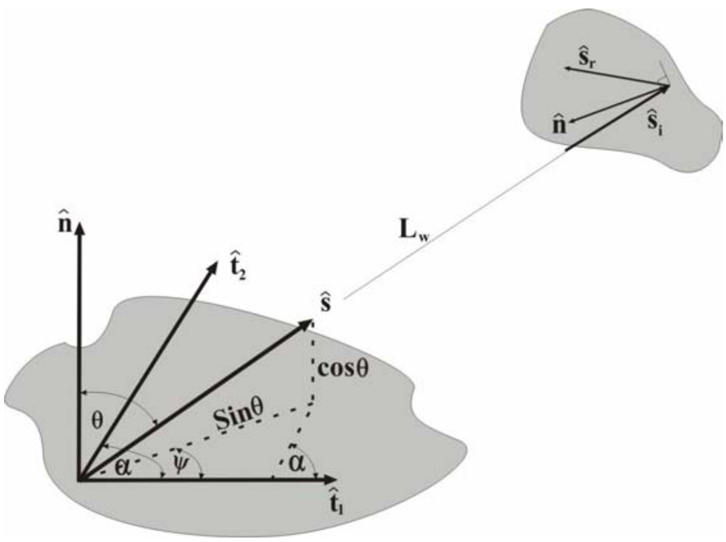

Figure 3-2 Vector description of emission direction and point of incidence (Modest [30])

Ray tracing Algorithm:

Assuming that medium is transparent, the point $\vec{r}$ on a surface that the photon bundle emitted at location $\vec{r}_e$ will collide with and the corresponding distance L_w that the photon bundle will travel before this collision, is found by using,

$$\vec{r}_e + L_w \hat{s} = \vec{r}_w \qquad (3.25)$$

When rectangular coordinate system is considered, Eq. (3.25) can be written in terms of x, y, z components and solved for L_w by forming the dot products with unit vectors of rectangular coordinate system, $\hat{i}$, $\hat{j}$, and $\hat{k}$,

$$L_w = \frac{x - x_e}{\hat{s}.\hat{i}} = \frac{y - y_e}{\hat{s}.\hat{j}} = \frac{z - z_e}{\hat{s}.\hat{k}} \qquad (3.26)$$

Eq. (3.26) is a set of three equations, in the three unknowns, L_w, and two of the coordinates, where the third coordinate is defined in terms of the other two by using the surface equation. If more than one intersection is a possibility (in the presence of convex surfaces, etc.), then the path lengths L_w, for all possibilities are determined, the correct one is the one that gives the shortest possible path.

Having the wave number evaluated, the mean free path which is the distance that a photon bundle will travel before being absorbed by the gas medium, for the case in which the absorption coefficient does not vary throughout the medium (κ_η=constant), can be calculated by using,

$$L_\kappa = \frac{1}{\kappa_\eta} \ln\left(\frac{1}{R_\kappa}\right) \qquad (3.27)$$

If the absorption coefficient is not uniform, which can be due to temperature dependence or anisotropic medium, the optical path is evaluated by breaking up the volume into n sub-volumes each with a constant absorption coefficient.

$$\int_0^l \kappa_\eta ds \cong \sum_n \kappa_{\eta n} l_n \tag{3.28}$$

The summation in Eq. (3.28) is over the n sub-volumes through which the bundle has traveled, and l_n is the distance the bundle travels through in element n. The bundle is not absorbed and is allowed to travel on as long as the following condition holds,

$$\int_0^l \kappa_\eta dl < \int_0^{L_\kappa} \kappa_\eta dl = \ln \frac{1}{R_\kappa} \tag{3.29}$$

If the scattering coefficient does not vary throughout the medium, the distance that a photon bundle will travel before it is scattered can be evaluated by using,

$$L_\sigma = \frac{1}{\sigma_\eta} \ln\left(\frac{1}{R_\sigma}\right) \tag{3.30}$$

For a medium with variable scattering coefficient, the following condition holds:

$$\int_0^l \sigma_\eta dl \cong \sum_n \sigma_{\eta n} l_n < \int_0^{L_\sigma} \sigma_\eta dl = \ln \frac{1}{R_\sigma} \tag{3.31}$$

After having all L_κ, L_σ, and L_w in one hand, the three lengths can be compared to understand whether the bundle will be scattered by the gas, absorbed in the gas, or hits a wall. If L_w is the smallest of all, the bundle directly collides with the wall without being scattered or absorbed by the gas. Then, the absorptivity of the wall is compared with a generated random number. If the random number is smaller than the absorptivity, the wall absorbs the bundle. Otherwise, the bundle is reflected from the wall. If the surface is a diffuse reflector, angles of reflection can be calculated from the following expressions:

$$\theta_r=\arcsin(\sqrt{R\theta_r}) \tag{3.32}$$

$$\psi_r=2\pi R_{\psi_r} \tag{3.33}$$

If L_κ is the smallest, the gas absorbs the bundle. On the other hand, when L_σ is smaller than L_κ and L_w the bundle is scattered in the gas. Once a photon is scattered, it will travel on into a new direction as shown in Fig. 3-3. The new direction of the bundle can be determined by using the random number relations for the scattering angles. For anisotropic scattering, the cumulative distribution functions for polar and azimuthal scattering angles are obtained by evaluating the following integrals, respectively:

$$R_\psi=\frac{\int_0^{\psi'}\int_0^{\pi}\Phi(\hat{s}\cdot\hat{s}')\sin\theta'd\theta'd\psi'}{\int_0^{2\pi}\int_0^{\pi}\Phi(\hat{s}\cdot\hat{s}')\sin\theta'd\theta'd\psi'} \tag{3.34}$$

$$R_\theta=\frac{\int_0^{\theta'}\Phi(\hat{s}\cdot\hat{s}')\sin\theta'd\theta'}{\int_0^{\pi}\Phi(\hat{s}\cdot\hat{s}')\sin\theta'd\theta'} \tag{3.35}$$

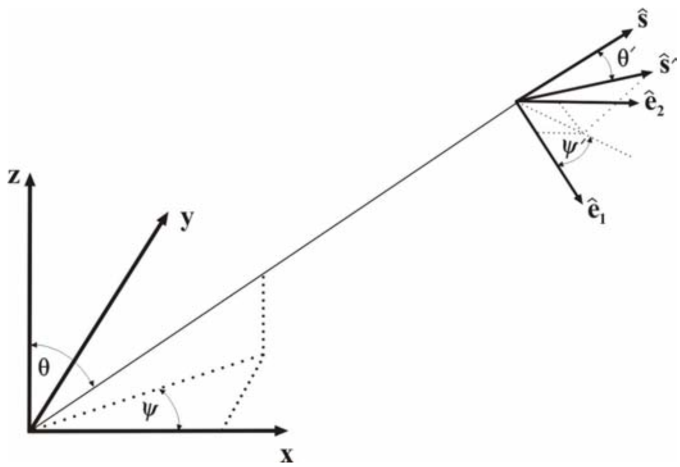

Fig. 3-3 Local coordinate system for scattering direction (Modest [30])

Φ is the scattering phase function in Eq. (3.34) and (3.35). For the case of isotropic scattering, $\Phi(\hat{s}\cdot\hat{s}') = 1$, and these relations become identical to those for emission, Eq. (3.12) and (3.20).

The point at which the bundle is scattered can be evaluated by using,

$$\vec{r} = \vec{r}_e + L_\sigma \hat{s} \tag{3.36}$$

At the point of scattering, as evaluated by Eq. (3.36), a new local coordinate must be set in order to trace the bundle in its new direction. When the local z-direction can be represented by $\hat{s}$, the local x-direction, $\hat{e}_1$ from which the azimuthal scattering angle ψ' is measured and the corresponding local y-direction, $\hat{e}_2$, are evaluated from the following expressions,

$$\hat{e}_1 = \frac{\vec{a} \times \hat{s}}{\left| \vec{a} \times \hat{s} \right|} \qquad (3.37)$$

$$\hat{e}_2 = \hat{s} \times \hat{e}_1 \qquad (3.38)$$

In Eq. (3.37), $\vec{a}$ is any arbitrary vector. Similar to Eq. (3.24), the new direction vector is expressed by

$$\hat{s}' = \sin\theta' [\cos\psi' \hat{e}_1 + \sin\psi' \hat{e}_2] + \cos\theta' \hat{s} \qquad (3.39)$$

Then, the new distance, L_w, that the bundle will travel before hitting a surface is evaluated from Eq. (3.26) by replacing the coordinates of point of emission by coordinates of point of scattering. The path that the bundle will travel before it is absorbed by gas, L_κ, can be calculated by reducing the traveled path from the value evaluated before. Based on the values obtained by a similar procedure, the photon bundle is traced until it hits a surface and absorbed by it, or until a gas volume absorbs it.

A similar ray tracing procedure continues until the gas or one of the surfaces absorbs the bundle, where the history is terminated. Then, a new history starts with the emission of a new bundle. The simulation continues until the whole energy that is generated and recovered in the system is considered.

CHAPTER 4

APPLICATIONS OF MONTE CARLO METHOD TO SURFACE EXCHANGE PROBLEMS

Monte Carlo method is first applied to surface exchange problems so that the general characteristics of the method can be understood in simpler problems before the method is applied to more complex problems involving three-dimensional geometries and participating media.

The surface exchange problems can be considered in two different categories. The first is evaluation of view factors of certain geometries and the second is evaluation of the net radiation exchange between a number of black and grey surfaces.

4.1 EVALUATION OF VIEW FACTORS

The view factor F_{ij} is defined as the fraction of radiation leaving surface i, which is intercepted by surface j. The general expression that gives the view factor for two surfaces that are diffuse emitters and reflectors and have uniform radiosity is given in Eq. (4.1),

$$F_{ij}=\frac{1}{A_i}\int_{A_j}\int_{A_i}\frac{\cos\theta_i\cdot\cos\theta_j}{\pi S^2}dA_i dA_j \tag{4.1}$$

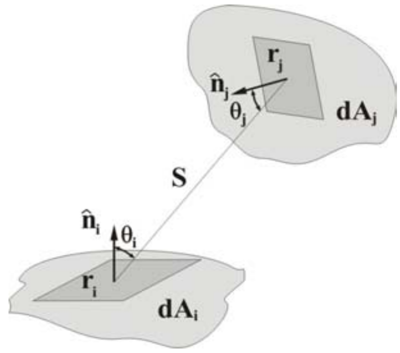

Figure 4.1 Radiative exchange between elemental surfaces of area dA_i, dA_j (Modest [30])

where θ_i, θ_j are the polar angles for surfaces i, j respectively and S is the distance between the surfaces as shown in Fig. 4.1.

For simple configurations, the integrals can be evaluated analytically. However, numerical methods must be used for more complex cases. Monte Carlo method can be used when complex geometries or further difficulties like non-diffuse emitters and reflectors are present in the problem.

The view factor of surface i to surface j can be evaluated by Monte Carlo method, i.e., emitting a number of photon bundles from surface i and counting the number of bundles hitting surface j. The ratio of number of photon bundles that hits surface j to the number of photon bundles that are emitted from surface i gives the view factor F_{ij}.

The view factors for three different configurations are evaluated by the Monte Carlo method and the results are compared with the results obtained from analytical formulations. Three configurations are selected such that the view factors are given by analytical formulas.

The first selected configuration is two aligned, parallel, equal rectangles as shown in Fig.4.2,

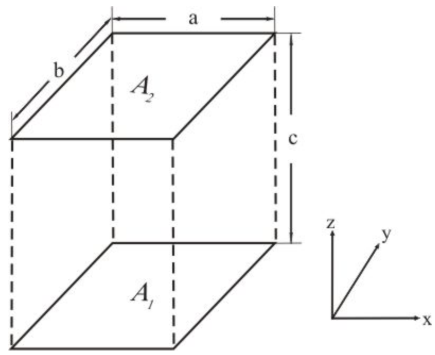

Figure 4.2 Two aligned, parallel, and equal rectangles (Modest [30])

The view factor F_{12} for the configuration under consideration is calculated by Monte Carlo method, and is compared with the analytical solution given by the following expression:

$$F_{12} = \frac{2}{\pi \overline{X}\overline{Y}} \left\{ \ln\left[\frac{(1+\overline{X}^2)\cdot(1+\overline{Y}^2)}{1+\overline{X}^2+\overline{Y}^2}\right]^{1/2} + \overline{X}(1+\overline{Y}^2)^{1/2}\tan^{-1}\left[\frac{\overline{X}}{(1+\overline{Y}^2)^{1/2}}\right] \right.$$

$$\left. + \overline{Y}(1+\overline{X}^2)^{1/2}\tan^{-1}\left[\frac{\overline{Y}}{(1+\overline{X}^2)}\right] - \overline{X}\tan^{-1}\overline{X} - \overline{Y}\tan^{-1}\overline{Y} \right\} \qquad (4.2)$$

In Eq. (4.2), $\overline{X} = a/c$ and $\overline{Y} = b/c$.

The points of emission are calculated by Eq. (3.9) and (3.10); the azimuthal and polar angles of the emitted photon bundles are obtained by Eq. (3.12), (3.13), respectively.

$$x_e = R_x.(a) \tag{4.3}$$

$$y_e = R_y.(b) \tag{4.4}$$

$$\psi = 2\pi R_\psi \tag{4.5}$$

$$\theta = \arcsin(\sqrt{R_\theta}) \tag{4.6}$$

where R_x, R_y, R_ψ, and R_θ are random numbers.

As the distance c is fixed, the points of the bundles passing through at the plane of surface 2 can be evaluated as,

$$x= x_e +c.\tan\theta.\cos\psi \tag{4.7}$$

$$y=y_e + c.\tan\theta.\sin\psi \tag{4.8}$$

where ψ is measured from positive x-axis and θ is measured from positive z-axis.

If x and y coordinates which are calculated by Eq. (4.7) and (4.8), are in the area bounded by surface 2, the counter for the hits on surface 2 is increased by one. After a number of photon bundles are emitted from surface 1, the view factor F_{12} can be evaluated.

The second configuration selected is perpendicular rectangles with an equal common edge as shown in Fig. 4.3.

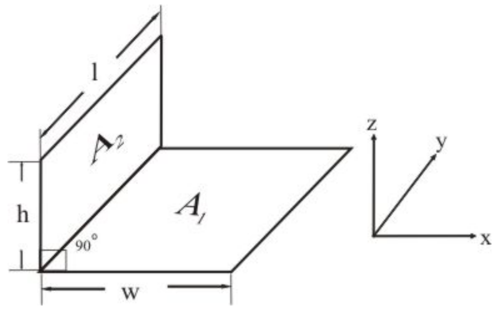

Figure 4.3 Perpendicular rectangles with an equal common edge (Modest [30])

The view factor F_{12} calculated by Monte Carlo method is compared with the analytical solution given by the following expression,

$$F_{12} = \frac{1}{\pi W}\left(W\tan^{-1}\frac{1}{W} + H\tan^{-1}\frac{1}{H} - (H^2 + W^2)^{1/2}\tan^{-1}\frac{1}{(H^2 + W^2)^{1/2}} \right.$$

$$\left. + \frac{1}{4}\ln\left\{ \frac{(1+W^2)(1+H^2)}{1+W^2+H^2}\left[\frac{W^2(1+W^2+H^2)}{(1+W^2)(W^2+H^2)}\right]^{W^2} \times \left[\frac{H^2(1+H^2+W^2)}{(1+H^2)(H^2+W^2)}\right]^{H^2} \right\} \right) \quad (4.9)$$

where H = h/l and W = w/l in Eq. (4.9).

The points of emissions from surface 1 are calculated by Eq. (3.9) and (3.10). The azimuthal and polar angles of the emitted photon bundles are obtained from Eq. (3.12), (3.13), respectively, just like the first case. This time, the x-coordinate of the plate 2 is fixed and the points of the bundles passing through at the plane of surface 2 can be evaluated by,

$$x_e = R_x.(w) \quad (4.10)$$

$$y_e = R_y.(l) \tag{4.11}$$

$$y = y_e - x_e \tan\psi \tag{4.12}$$

$$z = z_e - \left(\frac{x_e}{\tan\theta \cos\psi}\right) \tag{4.13}$$

As it is done in the first case, if y and z coordinates which are calculated by Eq. (4.12) and (4.13) are in the area bounded by surface 2, the counter of the hits on surface 2 is increased by one. After a number of photon bundles is emitted from surface 1, the view factor F_{12} can be evaluated.

The third configuration selected is parallel co-axial discs as shown in Fig. 4.4

The view factor F_{12} calculated by Monte Carlo method was compared with the analytical solution given by the following expression,

$$F_{12} = \frac{1}{2}\left[X - \sqrt{X^2 - 4\left(\frac{R_1}{R_2}\right)^2}\right] \tag{4.14}$$

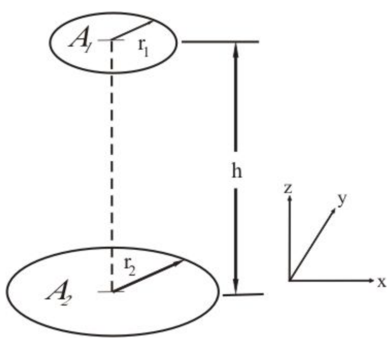

Figure 4.4 Parallel co-axial discs (Modest [30])

In Eq. (4.14), $R_1 = r_1 / h$, $R_2 = r_2 / h$ and $X = 1 + (1 + R^2{}_2) / R_1{}^2$.

The points of emission from surface 1 are calculated by Eq. (3.9), the azimuthal and polar angles of the emitted photon bundles are obtained by Eq. (3.12), (3.13), respectively. The points of locations of the bundles passing through at the plane of surface 2 can be evaluated by,

$$r_e = R_r.(r_1) \tag{4.14}$$

$$r = \sqrt{((h.\tan\theta)^2 + (r_e)^2 - 2.(r_e \cdot h \cdot \tan\theta \cdot \cos(\pi - \psi)))} \tag{4.15}$$

If r calculated by Eq. (4.15) is in the area bounded by surface 2, the counter of the hits on surface 2 is increased by one. After a number of photon bundles are emitted from surface 1, the view factor F_{12} can be evaluated.

Variance reduction can be applied to reduce computation time in each case by selecting azimuthal angles within range of interest between θ_{max} and θ_{min}, or ψ_{max} and ψ_{min}, instead of selecting θ between 0 and $\pi/2$ and ψ between 0 and 2π, respectively. Then, Eq. (3.12) and (3.13) used to define the direction of the emitted photon bundles become,

$$\psi = R_\psi (\psi_{max} - \psi_{min}) + \psi_{min} \tag{4.16}$$

$$\theta = \arcsin(\sqrt{R_\theta}(\sin^2\theta_{max} - \sin^2\theta_{min}) + \sin^2\theta_{min})) \tag{4.17}$$

The ratio of number of photon bundles that hits surface 2 to the number of photon bundles that is emitted from surface 1 is multiplied by $(\psi_{max} - \psi_{min})/2\pi$ when azimuthal angle is used with variance reduction, and is multiplied by $(\sin^2 \theta_{max} - \sin^2 \theta_{min})$ when polar angle is used with variance reduction, to obtain the view factor F_{12}.

The results obtained for the first configuration with and without variance reduction of polar angle for $\theta_{max} = \pi/4$ and $\theta_{min}=0$ are shown in Table 4.1 for a=1 cm, b=1 cm and c=1 cm for the dimensions given in Fig.4.2. The analytical result obtained from Eq. (4.2) is $F_{12} = 0.200$. Throughout this study, the true percent relative errors of a predicted value, $X_{predicted}$, are evaluated by using the following expression:

$$E=100.\frac{X_{exact} - X_{predicted}}{X_{exact}} \tag{4.18}$$

Table 4.1 The view factors and true percent relative errors for two aligned, parallel, equal rectangles evaluated by Monte Carlo method with and without variance reduction

No. of Histories	Without Variance Reduction		With Variance Reduction	
	F_{12}	E (%)	F_{12}	E (%)
100	0.150	-24.934	0.170	-14.926
1.000	0.198	-0.822	0.191	-4.234
10.000	0.200	-0.003	0.196	-1.806
100.000	0.199	-0.205	0.197	-1.392
1.000.000	0.200	-0.157	0.198	-1.011

The results obtained for the second configuration with and without variance reduction of polar angle for $\psi_{max}=3\pi/4$ and $\psi_{min}=\pi/2$ are shown in Table 4.2 for h = 1 cm, w = 1 cm and l = 1 cm for the dimensions given in Fig. 4.3. The analytical result obtained from Eq. (4.9) is $F_{12} = 0.200$.

Table 4.2 The view factors and true percent relative errors for perpendicular rectangles with an equal common edge evaluated by Monte Carlo method with and without variance reduction

No. of Histories	Without Variance Reduction		With Variance Reduction	
	F_{12}	E (%)	F_{12}	E (%)
100	0.220	9.976	0.228	13.863
1.000	0.209	4.523	0.204	1.786
10.000	0.198	-0.878	0.202	0.784
100.000	0.202	0.829	0.201	0.646
1.000.000	0.201	0.324	0.200	0.118

Similarly, the results obtained for the third configuration with and without variance reduction of polar angle for $\theta_{max}=\pi/3$ and $\theta_{min}=0$ are shown in Table 4.3 for D_1=1 cm, D_2=1 cm and h=1 cm for the dimensions given in Fig. 4.4. The analytical result obtained from Eq. (4.14) is F_{12} = 0. 192.

Table 4.3 The view factors and true percent relative errors for parallel co-axial discs evaluated by Monte Carlo method with and without variance reduction

No. of Histories	Without Variance Reduction		With Variance Reduction	
	F_{12}	E (%)	F_{12}	E (%)
100	0.120	30.059	0.174	-1.506
1.000	0.195	-13.389	0.165	3.852
10.000	0.178	-3.809	0.166	0.335
100.000	0.181	-5.410	0.165	0.374
1.000.000	0.180	-5.041	0.165	0.411

When we examine all the tables of results, it can be said that variance reduction produces results that are more accurate when small number of photon histories are used. However, Monte Carlo method without variance reduction also predicts accurate results when we use high number of photon histories.

Therefore, we can conclude that variance reduction is useful method when we use small N (# of photon bundle history). In addition, when one of the dimensions of the geometry is very small or greater than the other dimensions, variance reduction gives better results than without using variance reduction. On the other hand, there is a criterion for variance reduction. The determination of at what angles we are going to restrict the angles to hit the second surface is a critical issue, and it affects the results very significantly. Therefore, the angles must be chosen carefully when the variance reduction technique is used.

4.2 EVALUATION OF NET RADIATION EXCHANGE

If the two black surfaces in Fig. 4.1 is considered, the radiation leaving surface i and intercepted by surface j is,

$$q_{i\rightarrow j} = F_{ij}A_i\sigma T_i^4 \tag{4.19}$$

Similarly, the radiation leaving the surface j and intercepted by surface i is,

$$q_{j\rightarrow i} = F_{ji}A_j\sigma T_j^4 \tag{4.20}$$

From the reciprocity relation, it is known that,

$$A_iF_{ij} = A_jF_{ji} \tag{4.21}$$

Then, the net radiation exchange between the two black surfaces can be formulated as,

$$q_{ij}= q_{i\rightarrow j} - q_{j\rightarrow i} =F_{ij}A_i\sigma(T_i^4-T_j^4) \tag{4.22}$$

For simple geometric configurations and simple radiative properties such as black walls and diffuse emitters and reflectors, the problem of radiation exchange is simple and can be easily handled with analytical methods. But, when further complications arise such as complex geometries and non-grey or non-diffuse surfaces, numerical methods must be used.

Application of the Monte Carlo method to net radiation exchange problems is very similar to the application of the method for determination of the view factor problems. The main difference is, for the surface exchange problems, the photon bundles are considered to carry some amount of energy specified by Eq. (3.1). This energy is transmitted to the other surface when the emitted photon bundle hits a surface and is absorbed by that surface. The net radiative heat transferred to a surface can be found when all the surfaces emit some number of photon bundles with some energy assigned to each of the bundle, and calculating the difference between the energy emitted from the surface and energy absorbed by the surface.

4.3 EVALUATION OF NET RADIATION EXCHANGE BETWEEN BLACK SURFACES

The net radiation exchange problems are solved for the two rectangular box configurations as shown in Figs. 4.5 and 4.6, and the results obtained by using different numbers of photon bundle histories are compared with the results of analytical formulation.

Analytical solution of radiative heat exchange between isothermal black surfaces are obtained as,

$$q_i=\sum_{j=1}^{N} F_{i-j}\left(E_{bi}-E_{bj}\right)-H_{oi}\ , \qquad i=1,2,...,N. \qquad (4.23)$$

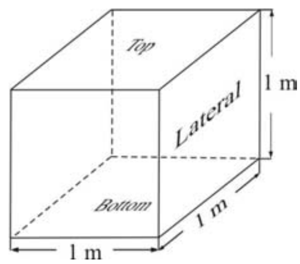

Figure 4.5 Configuration 1

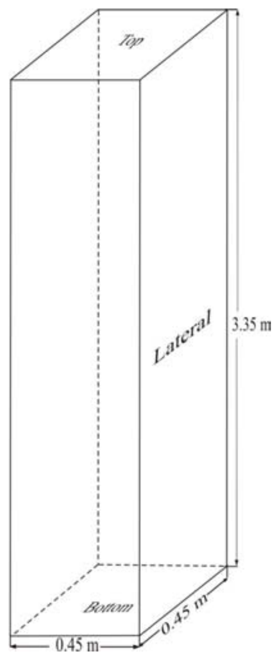

Figure 4.6 Configuration 2

During the solutions, the number of photon bundles emitted from each isothermal surface is kept constant while the energy of each emitted photon bundle is taken to be directly proportional to the emissive power of the point of emission. Based on this assumption, energy of the photon bundles emitted from each plate is directly proportional to the fourth power of the absolute temperature of the plate, evaluated from Eq. (3.1).

The net radiative heat exchange between the surfaces is calculated for the enclosures shown in Fig. 4.5 and 4.6. Temperature values of the surfaces are the same as the problems in participating medium that will be discussed in the following chapters. The solutions that are obtained with different number of histories are presented in Tables 4.4., 4.5 and 4.6 for T_{bottom}=1149 K, T_{top}=822 K and $T_{lateral}$=1059 K. The analytical results and true percent relative errors are obtained by Eq. (4.23) and Eq. (4.18), respectively.

Table 4.4 The net radiative heat exchange for bottom surface

No. of Histories from bottom surface	Bottom Surface			
	Configuration 1		Configuration 2	
	q_{exact}=3.56X10^4 W		q_{exact}=5.42X10^3 W	
	q_{MC}(W)	Err.(%)	q_{MC}(W)	Err.(%)
100	4.06 X10^4	-14.26	6.03 X10^3	-11.3
1.000	3.56 X10^4	0.01	4.52 X10^3	16.5
10.000	3.51 X10^4	1.37	5.10 X10^3	5.8
100.000	3.57 X10^4	-0.33	5.50 X10^3	-1.6
1.000.000	3.55 X10^4	0.31	5.40 X10^3	0.3

Table 4.5 The net radiative heat exchange for top surface

No. of Histories from top surface	Top Surface			
	Configuration 1		Configuration 2	
	q_{exact}=-5.07X10^4 W		q_{exact}=-9.23X10^3 W	
	q_{MC}(W)	Err.(%)	q_{MC}(W)	Err.(%)
100	-5.14 X10^4	-1.41	-4.43 X10^3	52.0
1.000	-4.75 X10^4	6.26	-6.07 X10^3	34.2
10.000	-5.11 X10^4	-0.75	-8.67 X10^3	6.0
100.000	-5.05 X10^4	0.49	-9.16 X10^3	0.8
1.000.000	-5.06 X10^4	0.18	-9.21 X10^3	0.2

Table 4.6 The net radiative heat exchange for lateral surface

No. of Histories from lateral surface	Lateral Surface			
	Configuration 1		Configuration 2	
	q_{exact}=1.52X10^4 W		q_{exact}=3.81X10^3 W	
	q_{MC}(W)	Err.(%)	q_{MC}(W)	Err.(%)
400	1.08 X10^4	28.7	-1.59 X10^3	141.8
4.000	1.19 X10^4	20.9	1.55 X10^3	59.4
40.000	1.60 X10^4	-5.73	3.57 X10^3	6.3
400.000	1.48 X10^4	2.43	3.65 X10^3	4.2
4.000.000	1.52 X10^4	-0.12	3.81 X10^3	0.1

From the results, it can be concluded that the Monte Carlo algorithms are validated for the simple view factor and radiative heat exchange problems. The verified algorithms can be modified for problems with more complex geometries and radiative problems, but as the aim of the study is to verify the method in three-dimensional enclosure problems containing participating medium, further modifications are made in that direction.

4.4 EVALUATION OF NET RADIATION EXCHANGE BETWEEN DIFFUSE GREY SURFACES

The net radiation exchange problems between isothermal black and grey surfaces are solved for box configurations as shown above in Fig. 4.5 and 4.6. The results obtained by using different numbers of photon bundle histories are compared with the results of analytical formulation. The flow chart of the MCM code is given in Appendix Fig.A1.

Analytical solution of radiative heat exchange between black and grey surfaces are obtained as,

$$\frac{q_i}{\varepsilon_i} - \sum_{j=1}^{N}\left(\frac{1}{\varepsilon_j} - 1\right)F_{i-j}q_j + H_{oi} = \sum_{j=1}^{N} F_{i-j}\left(E_{bi} - E_{bj}\right), \qquad i=1, 2,..., N \quad (4.24)$$

The net radiative heat exchange between the surfaces is calculated for the enclosures shown in Figs. 4.5 and 4.6. The solutions that are obtained with different number of histories are presented in Tables 4.7, 4.8 and 4.9 for T_{bottom}=1149 K, T_{top}=822 K and $T_{lateral}$=1059 K. The analytical results and true percent relative errors are obtained by Eq. (4.24) and Eq. (4.18), respectively.

Table 4.7 The net radiative heat exchange for bottom surface

No. of Histories from bottom surface	Bottom Surface			
	Configuration 1		Configuration 2	
	q_{exact}=1.04X10^4 W		q_{exact}=1.80X10^3 W	
	ε_1=0.33 ε_2=0.33 $\varepsilon_{lateral}$=0.33		ε_1=0.33 ε_2=0.33 $\varepsilon_{lateral}$=0.33	
	q_{MC}(W)	Err.(%)	q_{MC}(W)	Err.(%)
100	4.87X10^3	53.0	-6.80X10^2	137.7
1.000	9.56X10^3	7.6	1.04X10^3	42.5
10.000	9.92X10^3	4.1	1.47X10^3	18.7
100.000	1.00X10^4	3.0	1.58X10^3	12.5
1.000.000	1.01X10^4	2.7	1.62X10^3	10.1

Table 4.8 The net radiative heat exchange for top surface

No. of Histories from top surface	Top Surface			
	Configuration 1		Configuration 2	
	q_{exact}=-1.48X10^4 W		q_{exact}=-3.01X10^3 W	
	ε_1=0.33 ε_2=0.33 $\varepsilon_{lateral}$=0.33		ε_1=0.33 ε_2=0.33 $\varepsilon_{lateral}$=0.33	
	q_{MC}(W)	Err.(%)	q_{MC}(W)	Err.(%)
100	-1.15X10^4	22.0	-4.57X10^3	51.9
1.000	-1.42X10^4	4.1	-2.75X10^3	8.7
10.000	-1.44X10^4	2.4	-2.85X10^3	5.4
100.000	-1.44X10^4	2.1	-2.73X10^3	9.2
1.000.000	-1.45X10^4	1.7	-2.78X10^3	7.9

Table 4.9 The net radiative heat exchange for lateral surface

No. of Histories from lateral surface	Lateral Surface			
	Configuration 1		Configuration 2	
	q_{exact}=4.41X10^3 W		q_{exact}=1.21X10^3 W	
	ε_1=0.33 ε_2=0.33 $\varepsilon_{lateral}$=0.33		ε_1=0.33 ε_2=0.33 $\varepsilon_{lateral}$=0.33	
	q_{MC}(W)	Err.(%)	q_{MC}(W)	Err.(%)
400	6.64X10^3	-50.7	5.25X10^3	-334.5
4.000	4.59X10^3	-4.2	1.71X10^3	-41.8
40.000	4.49X10^3	-1.8	1.38X10^3	-14.4
400.000	4.41X10^3	0.1	1.16X10^3	4.4
4.000.000	4.44X10^3	-0.7	1.15X10^3	4.7

When we examine the net radiative heat exchange between the surfaces inside the rectangular enclosure, it can be seen from the tables that Monte Carlo method gives accurate results for a cubic enclosure. However, the results for Configuration 2 (Fig. 4.6) are not as accurate as that of a cubic enclosure.

The photons emitted from and absorbed at the bottom and top surfaces have important weight in the solution. The reflectivity (ρ) values of opaque and diffuse walls are equal to (1-α) where α (absorptivity) equals to ε (emissivity) value. Low emissivity values leads to high reflectivity values. Therefore, emitted photons make high number of reflections in the enclosure because of low emissivity values of the walls. Then, high reflections of the photons in the enclosure and thin-long geometry of the configuration 2 affect the number of photons absorbed at the bottom and top surfaces. Smaller or larger number of absorptions at the walls than the expected is the main reason of high error values at the top and bottom surfaces. In Fig. 4.8, total number of histories emitted from the walls is kept constant, while ε values of the walls are changed to see the effect of high reflections on the results.

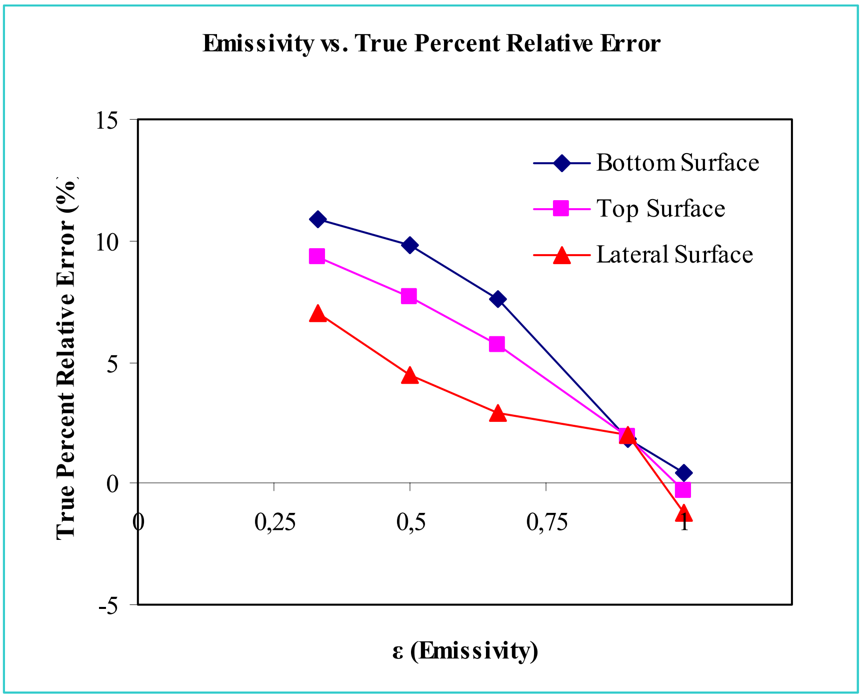

Figure 4.7 Comparisons of error by ε value

When the ε value of the wall is increased, the error of radiative exchange between the walls is decreased.

In our real problem, the bottom surface is black. Lateral and top surfaces are grey. The solution of Monte Carlo Method for this case is given in Table 4.10.

Table 4.10 The net radiative heat exchange for real problem

Total no. of history used in the enclosure	Configuration 2					
	ε_1=1.0		ε_2=0.87		$\varepsilon_{lateral}$=0.33	
	Bottom Surface		Top Surface		Lateral Surface	
	q_{exact}=5.57X10^3 W		q_{exact}=-7.89X10^3 W		q_{exact}=2.33X10^3 W	
	q_{MC}(W)	Err(%)	q_{MC}(W)	Err(%)	q_{MC}(W)	Err(%)
1.312.141	4.09X10^3	26.6	-6.26X10^3	20.7	2.17X10^3	6.5
13.121.417	4.12X10^3	26	-6.28X10^3	20.4	2.16X10^3	7.1
350.000.000	4.17X10^3	26	-6.28X10^3	20.4	2.17X10^3	6.9

In order to decrease the error, variance reduction technique is applied to the enclosure. The number of emitted photons is proportional to the area of the surface when we use uniform distribution of point of emission.

The volume near the bottom and top has important weight in the solutions. Near the bottom, the bottom surface absorbs larger number of photons than expected. Moreover, the top surface absorbs a smaller number of photons than expected due to the thin-long geometry of the enclosure as shown in Fig. 4.6 and high reflections in the enclosure. The photons, which are emitted from the top, bottom and lateral surfaces, are confined in the lateral zone and have little chance to go to the top and bottom surfaces. In order to eliminate this problem, biasing is used instead of direct simulation. The number of photons emitted from important regions is increased.

The lateral zone is divided into three parts as shown in Fig. 4.9. For two situations, the properties of the lateral zones are given in Table 4.11. The definitions of AR_x and PR_x, which are used in Table 4.11, are,

$$AR_x = \frac{\text{Area of lateral zone X}}{\text{Area of lateral surface}} \tag{4.25}$$

$$PR_x = \frac{\text{Total \# of emitted photons from lateral zone X}}{\text{Total \# of emitted photons from lateral surface}} \tag{4.26}$$

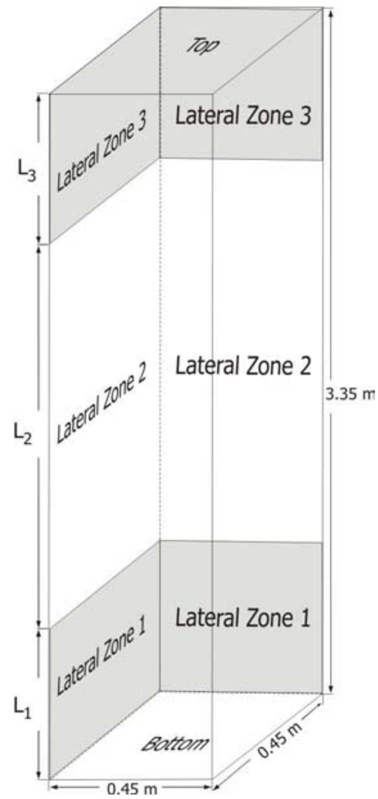

Figure 4.8 Lateral surface in three zones

Table 4.11 The lateral zone area and total number of emitted photons ratios for biasing

AR_1	PR_1	AR_2	PR_2	AR_3	PR_3
Biasing # 1 L_1=0.45 m L_2=2.45 m L_3=0.45 m					
13.43	10.00	73.14	72.50	13.43	17.50
Biasing # 2 L_1=0.90 m L_2=1.55 m L_3=0.90 m					
26.87	15.75	46.26	56.15	26.87	28.1

The net radiative heat exchange is analyzed for the problems under consideration. As the bottom surface absorbs a larger number of photons than expected, total emitted number of photons from lateral zone 1 is decreased. Similarly, emitted number of photons from lateral zone 3 is increased because the top surface absorbs a smaller number of photons than expected.

Table 4.12 Biasing #1

Total no. of history used in the enclosure	ε_1=1.0	ε_2=0.87	$\varepsilon_{lateral}$=0.33
	Bottom Surface	Top Surface	Lateral Surface
	Error (%)	Error (%)	Error (%)
2.500.000	-0.55	-0.62	-0.76
3.000.000	-0.77	-0.10	1.52
15.000.000	-0.76	-0.28	0.86

Table 4.13 Biasing #2

Total no. of history used in the enclosure	ε_1=1.0	ε_2=0.87	$\varepsilon_{lateral}$=0.33
	Bottom Surface	Top Surface	Lateral Surface
	Error (%)	Error (%)	Error (%)
1.000.000	2.08	0.90	-1.93
2.500.000	1.28	0.27	-2.17
3.000.000	0.70	0.42	-0.26

When we examine Tables 4.12 and 4.13, we may conclude that biasing produces good results. By increasing the number of photons emitted from zone 3, the number of absorbed photons at the top surface is increased. On the contrary, by decreasing the number of photons emitted from zone 1, the number of absorbed photons at the bottom surface is decreased.

The geometry of the enclosure is difficult for ray tracing applications. In order to eliminate this difficulty, biasing should be applied.

CHAPTER 5

APPLICATION OF MONTE CARLO METHOD TO PROBLEMS WITH PARTICIPATING MEDIUM

The difficulties in radiative transfer problems arise with interaction of thermal radiation with an absorbing, emitting and scattering medium. When participating medium is considered, the radiative transfer equation describes the radiative intensity field within the enclosure as a function of location, direction and spectral variable,

$$\hat{s}\cdot\vec{\nabla}I_\eta(\vec{r},\hat{s},\eta)=\kappa_\eta I_{b\eta}(\vec{r},\hat{s},\eta)-\beta_\eta I_\eta(\vec{r},\hat{s},\eta)+\frac{\sigma_{s\eta}}{4\pi}\int_{4\pi}I_\eta(\vec{r},\hat{s}',\eta)\Phi_\eta(\hat{s}',\hat{s})d\Omega' \tag{5.1}$$

where, I_η is the radiation intensity in the direction $\hat{s}$, at the position $\vec{r}$, defined as the quantity of radiant energy passing in specified direction $\hat{s}$ along a path per unit solid angle, per unit area normal to the direction of travel, per unit time. κ, σ_s and β are the absorption, scattering and extinction coefficients of the medium, respectively. $I_{b\eta}$ is the blackbody radiation intensity, and $\Phi_\eta(\hat{s}',\hat{s})$ is the scattering phase function, which describes the fraction of energy scattered from incoming direction $\hat{s}'$ to outgoing direction $\hat{s}$. The expression on the left-hand side represents the change of the intensity in the specified direction $\hat{s}$. The terms on the right-hand side stand for emission, extinction, and in-scattering, respectively.

In order to obtain the net radiation heat flux crossing a surface element, the contributions of radiative energy irradiating the surface from all possible directions and over all possible wave lengths must be summed up. Therefore, integrating the equation of transfer over all directions and all wave lengths leads to a conservation of radiative energy statement applied to an infinitesimal volume. It is impossible to handle these integrals by analytical means in most of the problems when the radiative properties are functions of location, direction and spectral variable at the same time.

When these difficulties arise coupled with multi-dimensional complex geometries, the approximate solution methods are used to evaluate the radiative heat fluxes subjected to the surfaces and divergence of radiative heat flux subjected to the medium. Monte Carlo method finds its main application area in problems of radiative transfer when participating medium and complex multi-dimensional geometries are considered.

In this study, the Monte Carlo method is applied to two enclosure problems to validate the accuracy. The first one is a 3-D cubical enclosure problem, which has numerical solutions [24]. The second one is a box-shaped enclosure problem. The comparisons will be made between experimental measurements and numerical solutions [26].

5.1 3-D CUBICAL ENCLOSURE PROBLEM CONTAINING SCATTERING MEDIUM

Most engineering problems are in fact non-ideal problems where simplifications are needed to obtain references to compare with the idealized cases and give rise to develop numerical solution techniques. The idealized problem studied in this part is a 3-D cubical enclosure containing uniform, grey, isotropically and anisotropically scattering medium bounded by diffuse, grey walls (Fig. 5.1). In this idealized problem, two cases are analyzed. The first cubical enclosure case is a purely scattering medium with non-symmetric boundary conditions. The second problem is characterized by an isothermal, absorbing, emitting, scattering medium and symmetric boundary conditions. The specified parameters of these problems are presented in Table 5.1. κ^*, σ_s^* and β^* are non-dimensional radiative properties defined as $\kappa^* = \kappa.L_o$, $\sigma_s^* = \sigma_s.L_o$, $\beta^* = \beta.L_o$ where L_o is the dimension of the cubical enclosure. The flow chart of the MCM code for this case is given in Appendix Fig.A2.

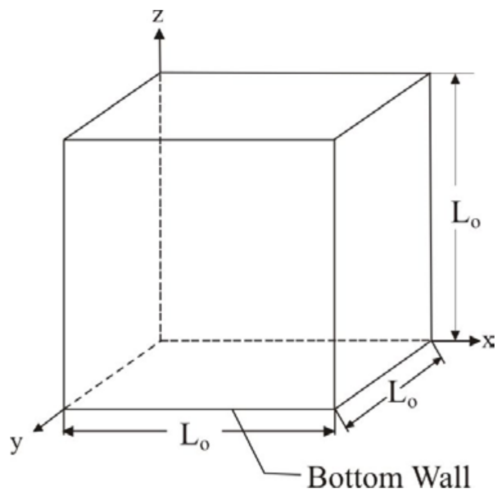

Fig. 5.1 Coordinate system for cubical enclosure problems [25]

Table 5.1 Input data for cubical enclosure problems [25]

Dimension of Cubical Enclosure, L_o		1.0 m	
Reference Temperature, T_o		648 K	
		Purely scattering medium with non-symmetric boundary conditions	Absorbing, emitting, scattering, medium with symmetric boundary conditions
Medium			
Scattering albedo, $\omega = \sigma_s^* / \beta^*$		1.0	0.5
Scattering coefficient, σ_s^*		1.0	5.0
Extinction coefficient, $\beta^* = \kappa^* + \sigma_s^*$		1.0	10.0
Temperature		0.0	T_o
Boundaries			
Temperature	z=0	T_o	0.0
	Others	0.0	0.0
Emissivity		1.0	1.0

These problems interested some researchers such as Kim and Huh [25]. They tested accuracies of various radiation models against Monte Carlo solutions in the form of a given non-dimensional radiative heat flux defined as

$$Q_i^* = \frac{q_i}{\sigma \cdot T_o^4} \tag{5.2}$$

where T_o is the reference temperature given in Table 5.1, and q_i represents the i-coordinate (x, y, and z) component of the radiative heat flux inside the medium given as

$$q_i = \int_{4\pi} (e_i \cdot \Omega) \cdot I \cdot d\Omega \quad (5.3)$$

where e_i is the unit normal vector in the coordinate direction i.

The scattering phase functions used to examine the effects of anisotropy in both problems are those given by Kim *et al.* [31]. The phase function $\Phi(\hat{s}', \hat{s})$, which represents the fraction of energy scattered into the outgoing direction $\hat{s}$ from the incoming direction $\hat{s}'$, is approximated by a finite series of Legendre polynomials as follows

$$\Phi(\hat{s}', \hat{s}) = \Phi(\text{Cos}\theta) = \sum_{j=0}^{N} C_j \cdot P_j(\text{Cos}\theta) \quad (5.4)$$

where P_j's are the Legendre polynomials of order j defined as

$$\begin{aligned} P_0 &= 1 \\ P_1 &= x \\ P_j &= \frac{2 \cdot j - 1}{j} \cdot x \cdot P_{j-1}(x) - \frac{j-1}{j} \cdot P_{j-1}(x) \end{aligned} \quad (5.5)$$

C_j's are the expansion coefficients and θ is the angle between incoming and outgoing directions.

Phase functions described by the expansion coefficients listed in Table 5.2 and illustrated in Fig. 5.2 are used in this study. The phase function F2 is for forward, and B2 is for backward scattering. Phase functions are shown in Figs. 5.3-5.5.

Table 5.2 Expansion coefficients for phase functions [31]

	C_j	
j	F2	B2
0	1.00000	1.00000
1	2.00917	-1.20000
2	1.56339	0.50000
3	0.67407	
4	0.22215	
5	0.04725	
6	0.00671	
7	0.00068	
8	0.00005	

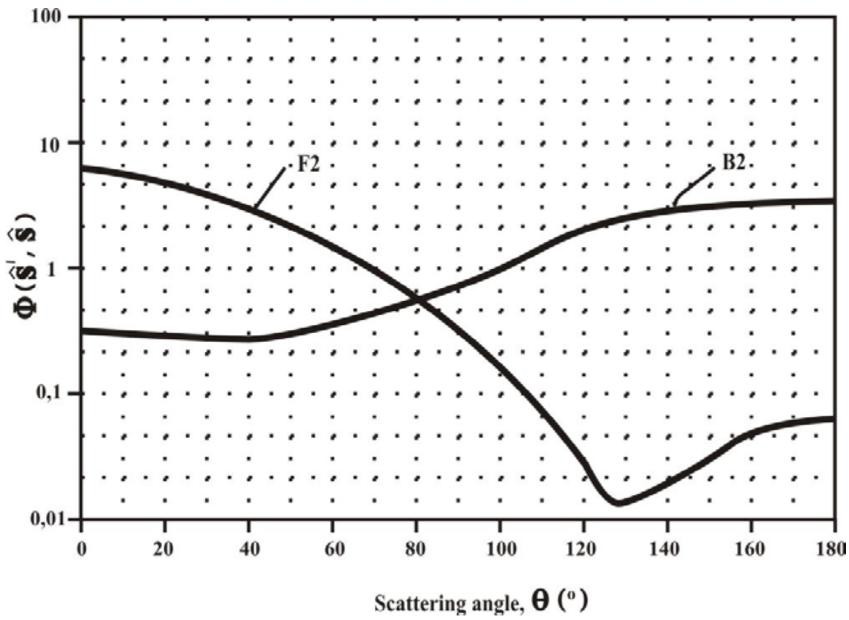

Fig. 5.2 Phase functions [31]

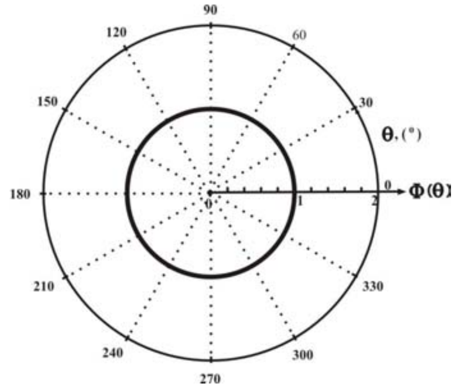

Fig. 5.3 Phase function for isotropic scattering [31]

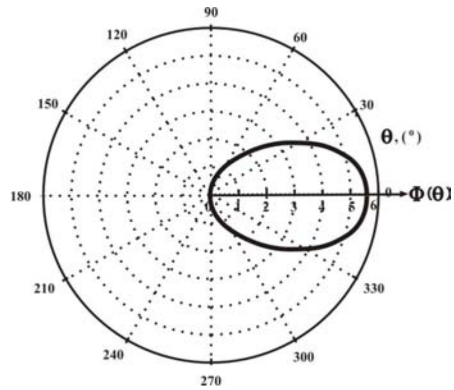

Fig. 5.4 Forward scattering phase function F2 [31]

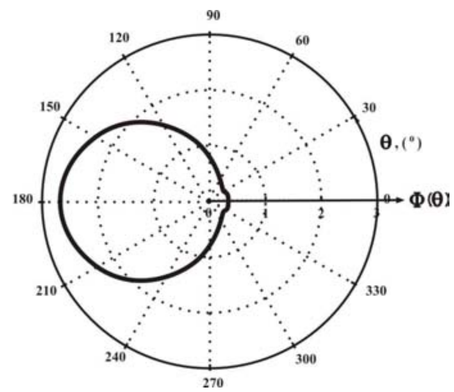

Fig. 5.5 Backward scattering phase function B2 [31]

5.2 FREEBOARD OF AN ATMOSPHERIC BUBBLING FLUIDIZED BED COMBUSTOR PROBLEM

The physical situation under consideration is the freeboard section of METU 0.3 MW_t Atmospheric Bubbling Fluidized Bed Combustor (ABFBC). The detailed description of the freeboard and properties of the participating medium are given in the references [24, 26, 27, 28, 29, 32, and 33].

As the problems are set to be more realistic and closer to the real engineering problems, the idealizations are lost and the approximate methods generally result in larger errors. However, some idealizing assumptions can still be made in most of the engineering systems. The freeboard is treated as a 3-D rectangular enclosure containing grey, absorbing, emitting, isotropically/anisotropically scattering medium with uniform radiative properties. The flow chart of the MCM code for the freeboard problem is given in Appendix Fig.A3.

5.2.1 Description of the Test Rig

The main body of the test rig is a modular combustor formed by five modules of 1 m height with internal cross-section of 0.45 m x 0.45 m. The first and the fifth modules refer to the bed and the cooler, respectively, and the three modules in between are the freeboard modules.

Temperature profiles of the wall and medium are reported by Selçuk [27], and given in Figure 5.6. There are two cooling surfaces of 0.35 m^2 and 4.3 m^2 in the bed and cooler modules as shown in Fig. 5.7, respectively.

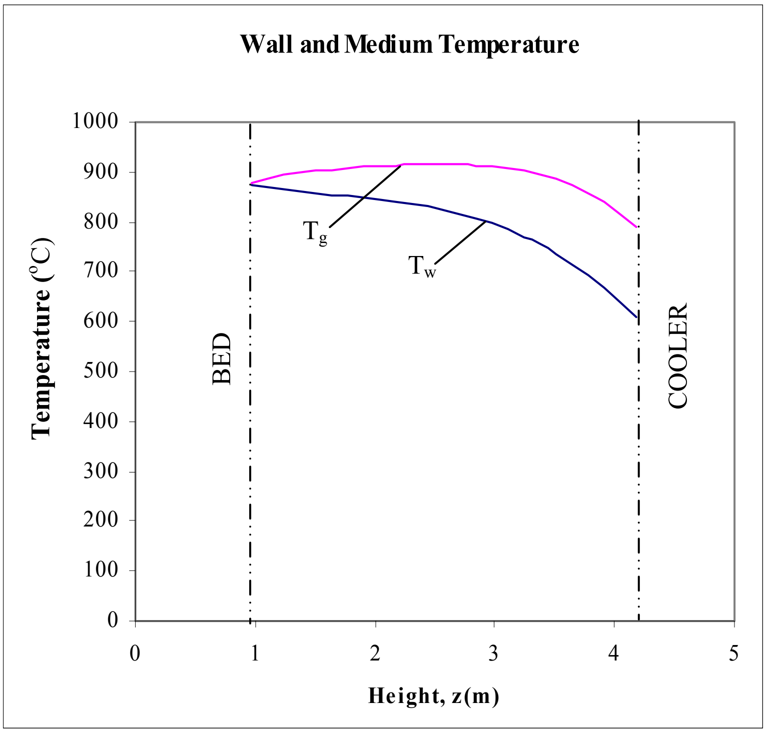

Polynomials for temperature profiles;

T_g=-5.2962 z^4+43.956 z^3-146.52 z^2+240.79 z+ 748.6 [°C]

T_w=-11.164 z^3+54.123 z^2-109.95 z+938.8 [°C]

Fig. 5.6 Temperature profiles along the freeboard [27]

5.2.2 Approximation of the ABFBC Freeboard as a 3-D Radiation Problem

In order to apply the radiation models to the freeboard, it is required to provide temperatures and radiative properties of the surfaces and the medium. The freeboard section of the combustor is treated as 3-D enclosure containing grey, absorbing, emitting and isotropically/anisotropically scattering medium bounded by diffuse, grey/black walls. The cooler boundary at the top, which consists of gas lanes and cooler tubes, is represented by an equivalent grey surface. The boundary with the bed section at the bottom is represented as a black surface. The physical system and the treatment of the freeboard are schematically shown in Fig. 5.7.

Radiative properties of the particle laden combustion gases and radiative properties and temperatures of the bounding surfaces are summarized in Table 5.3. These data together with medium and sidewall temperature profiles given in Fig.5.6 provide the input data supplied to the radiation models.

Table 5.3 Radiative properties of the medium and the surfaces [27]

Gas absorption coefficient, κ_g (1/m)	0.43
Absorption coefficient of particle cloud, κ_p (1/m)	0.16
Scattering coefficient of particle cloud, σ_s (1/m)	0.45
Extinction coefficient of the particles, $\beta_p= \kappa_p+ \sigma_s$ (1/m)	0.61
Absorption coefficient of the medium, $\kappa= \kappa_p+\kappa_g$ (1/m)	0.59
Extinction coefficient of the medium, $\beta= \kappa+ \sigma_s$ (1/m)	1.04
Scattering albedo of the medium, $\omega= \sigma_s/ \beta$	0.43
Emissivity of top surface, ε_{top}	0.87
Emissivity of side surfaces, ε_w	0.33
Emissivity of bottom surface, ε_{bottom}	1.00
Temperature of top surface (^oC), T_{top}	549
Temperature of bottom surface (^oC), T_{bottom}	873

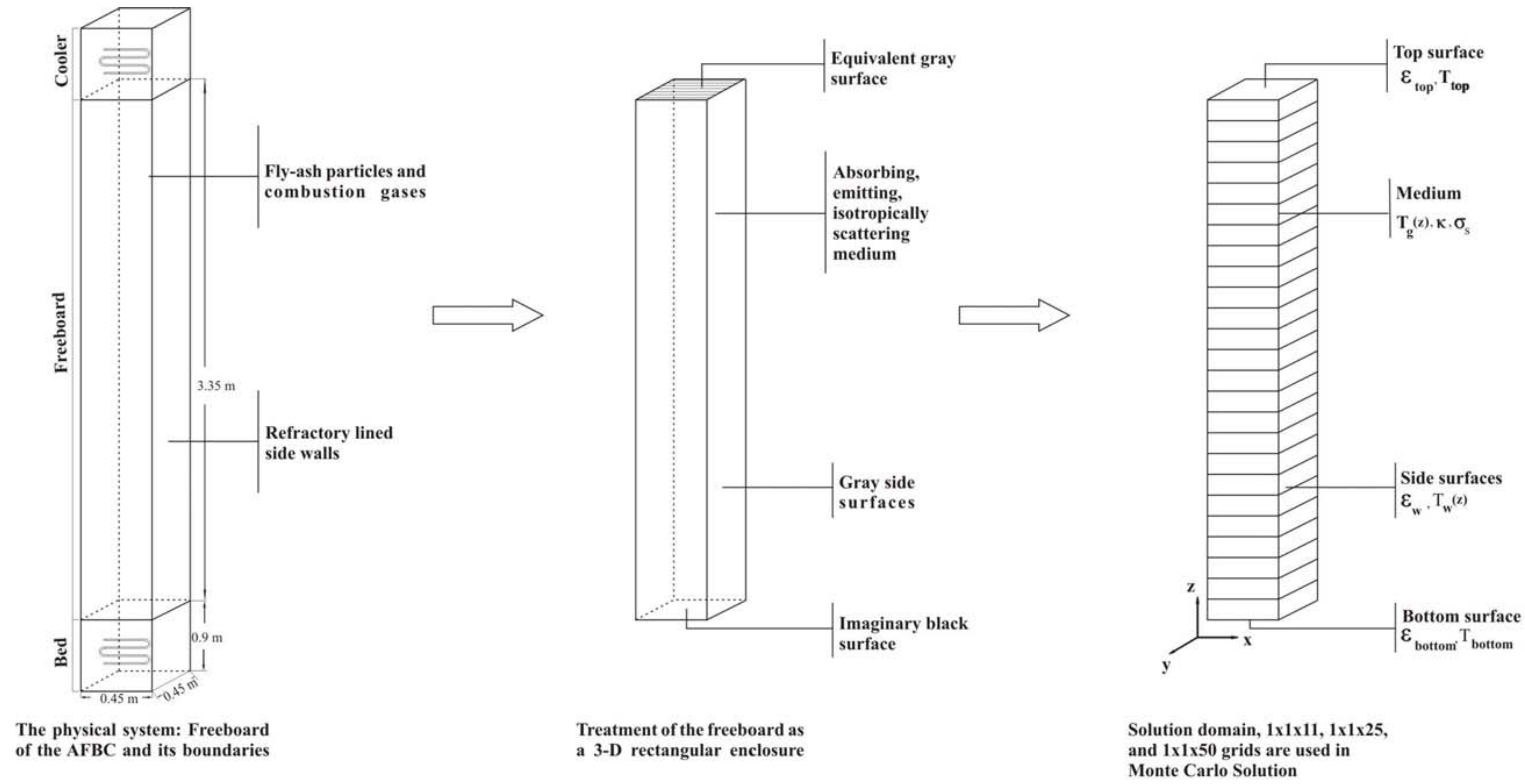

Fig. 5.7 Treatment of freeboard as a 3-D enclosure and solution domain for Monte Carlo Method [27]

CHAPTER 6

RESULTS AND DISCUSSION

The accuracy of the Monte Carlo method is examined by applying it to the enclosure problems described in Chapter 5. Based on the results and comparisons with the MOL of DOM solution of the same problems, it is possible to comment on the accuracy and computational efficiency properties of the MCM used for the problems under consideration.

In all cases, a computer, which has Intel Celeron 300 MHz processor and double precision of a FORTRAN compiler, is used.

6.1 3-D CUBICAL ENCLOSURE PROBLEM CONTAINING SCATTERING MEDIUM

In this part, the 3-D cubical enclosure problems, containing a scattering medium, are investigated. The physical system is a uniform, grey, purely scattering or absorbing, emitting and scattering medium bounded by diffuse, grey walls. Isotropic and anisotropic conditions are analyzed.

Accuracy of MCM is tested by applying it to the two problems described in Section 5.1 and comparing the predicted radiation variables against MOL of DOM solutions by Ayrancı [24]. The effect of the total number of photon histories used in MCM is investigated on the problem containing purely, isotropically scattering medium with non-symmetric boundary conditions. The parameters selected from this study are utilized in the calculation of the same problem with anisotropy and in the second problem with absorbing, emitting, and scattering problem.

In the cases that follow, the dimensionless radiative heat flux, Q_i^* as given in Eq. (5.2) is used for comparative purposes with the available MOL of DOM [24] solutions. The radiative heat flux along the i-coordinate, q_i is calculated by MCM as,

$$q_i = \sum_{n=1}^{M} \frac{[ni - nl] \cdot w \cdot \hat{s}_i}{A_n} \tag{6.1}$$

where, ni is the total number of incident photons on the surface or sub-volume, nl is the number of leaving photons from the surface or sub-volume, w is the photon energy, $\hat{s}_i$ is the direction cosine along the i-coordinate, A_n is the surface area normal to the i-coordinate, and finally M is the total number of photons emitted in the enclosure.

6.1.1 PURELY SCATTERING WITH NON-SYMMETRIC BOUNDARY CONDITIONS

MCM solution of this problem is investigated by comparing its predictions for radiative heat flux Q_z^* along the centerline of the enclosure ($L_o/2$, $L_o/2$, z) with those of MOL of DOM solutions obtained by dividing the enclosure into 25x25x25 sub-volumes using S_{10} order of approximation with LSO (Level Symmetric Odd) quadrature and DSS012 spatial discretization scheme [24].

The effect of grid spacing on the accuracy of MCM is investigated for this problem. The comparisons between the predictions of heat fluxes along the centerline with 1x1x25, 25x25x25 subdivisions of MCM and MOL of DOM are shown in Fig. 6.1. 62.5E6 photon bundles are used in the calculations. As can be seen from the figure, a satisfactory agreement is achieved by a finer grid spacing. 25X25X25 subdivision of grid spacing is selected for the following studies.

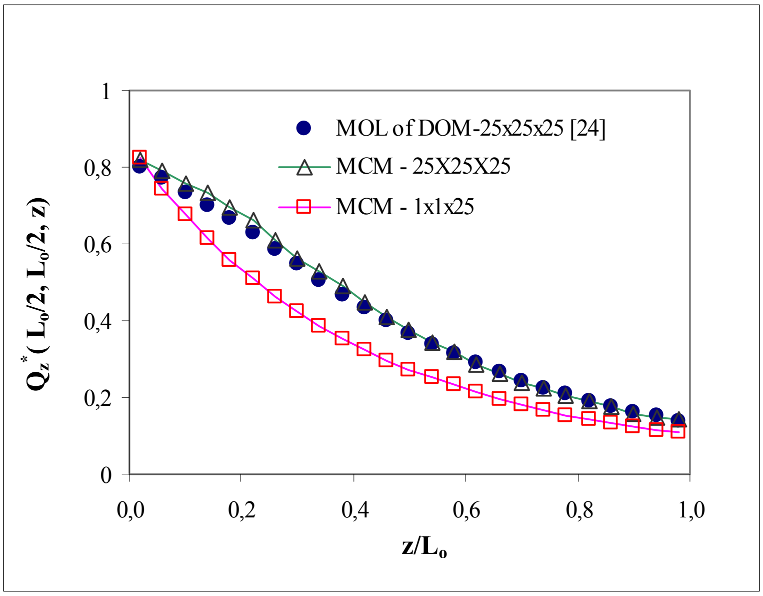

Fig. 6.1 Effect of grid spacing on the dimensionless heat flux predictions of Monte Carlo method

The effect of total number of photons used in MCM on the predictions is studied by running the program for 6.25E6, 62.5xE6 and 625XE6 photon bundles. We can conclude from Fig. 6.2 that increasing the total number of photon history affected the solution considerably. The predicted values oscillate if total number of photons is not enough. We can obtain good accuracy with a higher number of photon histories. Therefore, the effect of subdivision and total number of photon histories are the important parameters in this problem.

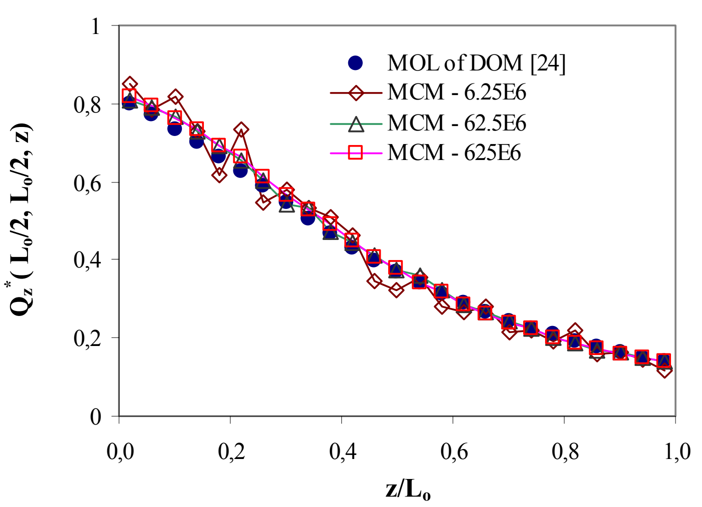

Fig. 6.2 Effect of total number of photons on the dimensionless heat flux predictions of Monte Carlo method

Having selected the grid spacing to 25x25x25 subdivision, MCM is applied to the prediction of dimensionless heat flux distributions along the centerline of the enclosure for anisotropically scattering media with forward and backward scattering phase functions as described in Section 5.1. Figs. 6.3 – 6.5 display the comparison between the MCM predictions and MOL of DOM solutions for the isotropically and anisotropically scattering cases, with phase functions F2 and B2, respectively. In all cases, 25x25x25 sub-volume and 62.5E6 photon bundles are used.

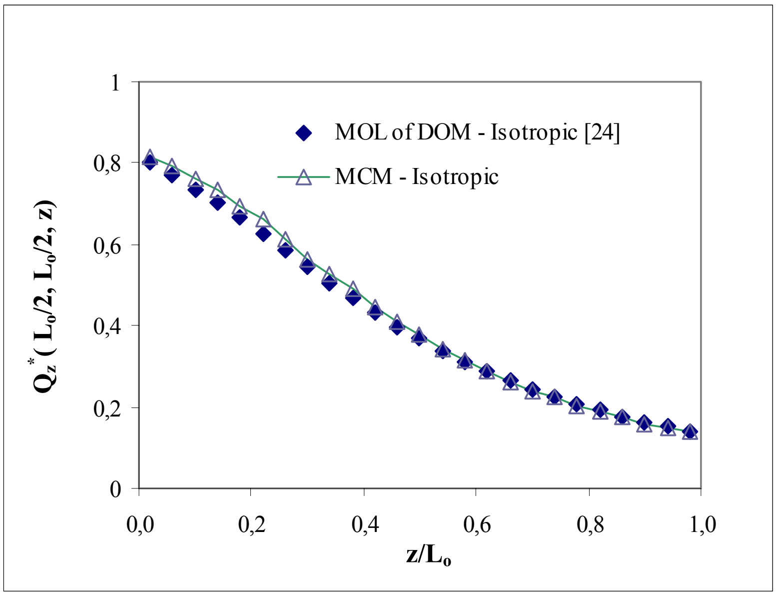

Fig. 6.3 Comparison between predictions of Monte Carlo method and MOL of DOM for dimensionless heat flux profiles along the centerline for isotropically scattering medium

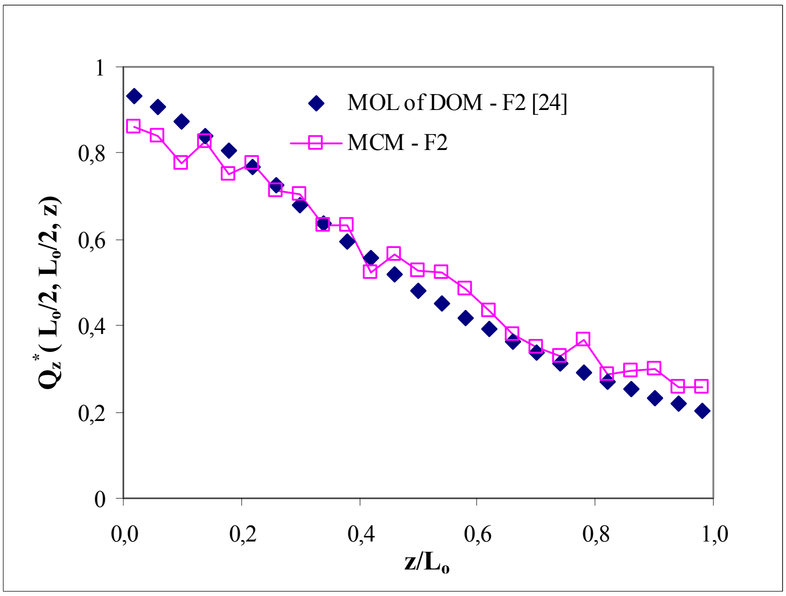

Fig. 6.4 Comparison between predictions of Monte Carlo method and MOL of DOM for dimensionless heat flux profiles along the centerline for anisotropically scattering medium with phase function F2

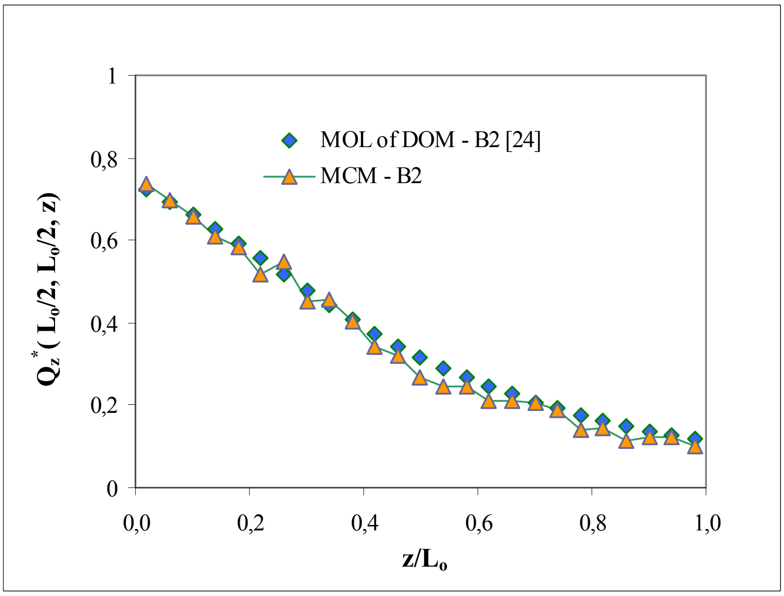

Fig. 6.5 Comparison between predictions of Monte Carlo method and MOL of DOM for dimensionless heat flux profiles along the centerline for anisotropically scattering medium with phase function B2

Table 6.1 Comparative testing between dimensionless heat flux predictions of Monte Carlo method and MOL of DOM [24] for various phase functions

Phase function	*Average absolute percentage error	Maximum absolute percentage error	CPU Time, s
Isotropic**	1.47	4.44	466.5
F2**	6.57	27.5	3262.6
B2**	6.69	22.2	887.5

$$^{*}\text{Absolute Percentage Error} = \left| \left(Q_{MCM}^{*} - Q_{\text{MOL of DOM}}^{*} \right) / Q_{\text{MOL of DOM}}^{*} \right| \cdot 100$$

**62.5E6 photon bundles are used

As can be seen from the above figures, the MCM solution in isotropic scattering medium agrees well with the MOL of DOM solutions, however there are oscillations in the predictions of F2 and B2 anisotropic scatterings. The grid spacing is insufficient to eliminate the oscillations. The grid spacing may be increased in further studies.

6.1.2 ABSORBING, EMITTING, SCATTERING MEDIUM WITH SYMMETRIC BOUNDARY CONDITIONS

The performance of MCM for this problem was investigated by comparing its predictions for dimensionless radiative heat flux Q_z^* along the centerline of a wall $(x, L_o/2, L_o)$ with those of MOL of DOM [24] obtained by dividing the enclosure into 25x25x25 sub-volumes, DSS012 scheme, S_{10} order of approximation. In all cases, 25x25x25 sub-volume and 62.5E6 photon bundles are used. Figures 6.6-6.8 illustrate the heat flux predictions of MCM and MOL of DOM for various phase functions.

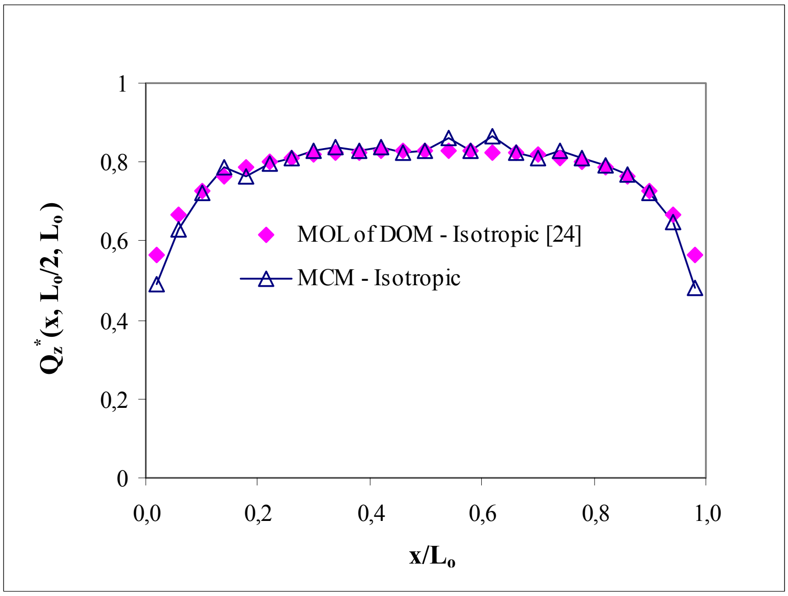

Fig. 6.6 Comparison between predictions of Monte Carlo method and MOL of DOM for dimensionless heat flux profiles along the x-axis for isotropically scattering medium

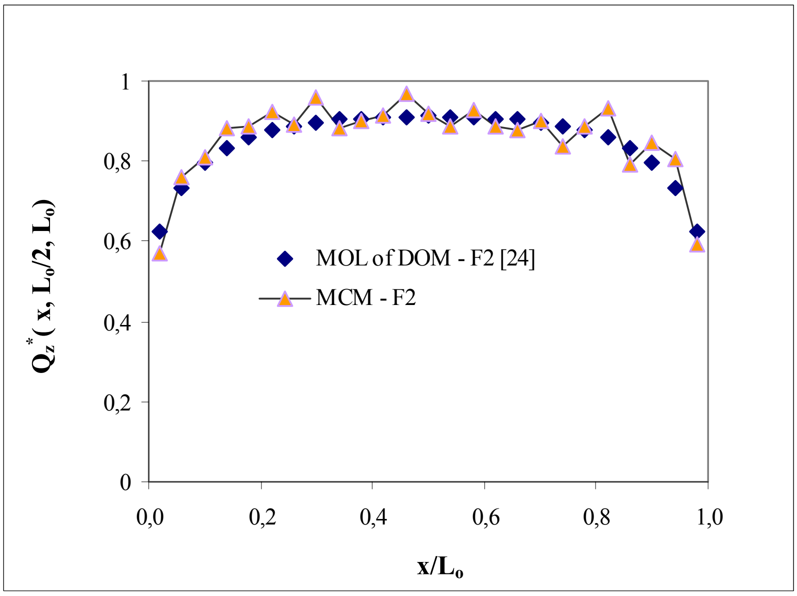

Fig. 6.7 Comparison between predictions of Monte Carlo method and MOL of DOM for dimensionless heat flux profiles along the x-axis for anisotropically scattering medium with phase function F2

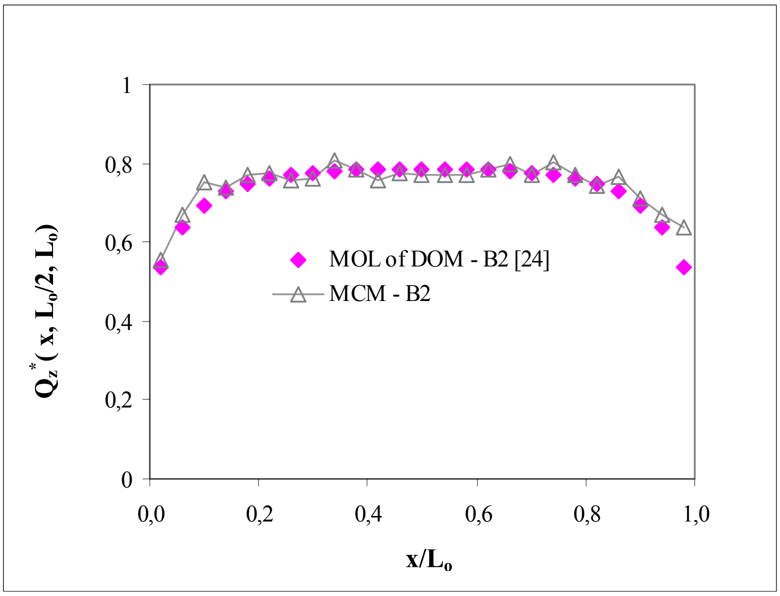

Fig. 6.8 Comparison between predictions of Monte Carlo method and MOL of DOM for dimensionless heat flux profiles along the x-axis for anisotropically scattering medium with phase function B2

The differences between the MCM and MOL of DOM are given in Table 6.2. As can be seen from the figures and table, MCM predictions are in reasonable agreement with those of MOL of DOM for isotropic scattering.

The grid spacing or the total number of photons emitted from the enclosure is insufficient to eliminate the oscillations in anisotropic scattering.

Table 6.2 Comparative testing between dimensionless heat flux predictions of Monte Carlo method and MOL of DOM [24] for various phase functions

Phase function	Average absolute percentage error*	Maximum absolute percentage error	CPU Time, s
Isotropic**	0.66	13.64	2742.6
F2**	1.82	13.94	13374.2
B2**	1.91	18.38	9155.5

*Absolute Percentage Error= $\left|\left(Q_{MCM}^{*} - Q_{MOL\ of\ DOM}^{*}\right)/\,Q_{MOL\ of\ DOM}^{*}\right| \cdot 100$

**62.5E6 photon bundles are used

6.2 FREEBOARD OF AN ATMOSPHERIC BUBBLING FLUIDIZED BED COMBUSTOR

The freeboard section of the 0.3 MW_t ABFBC is treated as a rectangular enclosure with diffuse, grey walls containing an absorbing, emitting, isotropically scattering medium. The predictive accuracy of MCM is assessed by applying it to the prediction of incident radiative fluxes on the freeboard walls of the combustor, and comparing its predictions with those of MOL of DOM and measurements.

6.2.1 Grid Refinement Study

The numerical accuracy and computational economy of the MCM with respect to grid spacing are investigated. The results are tabulated in Table 6.3. It can be concluded from Table 6.3 that errors decrease with number of grids at the expense of computational time. The use of 1x1x25 control volumes is found to be sufficient for this problem by considering the accuracy and computational economy.

Table 6.3 Grid refinement study for Monte Carlo method

Number of Control Volumes	Error* (%)	CPU time**, s
1x1x11	0.777	161.8
1x1x25	0.038	173.9

Reference case:1x1x50

*Error (%): Average percent relative error for predicted incident heat fluxes at grid points with respect to the predictions of the reference case.

**CPU time for the reference case is, 198.2 s for 4.2E6 total number of photon histories

6.2.2 Validation of MCM

Fig. 6.9 shows comparisons between the incident radiative heat fluxes predicted by MCM with the MOL of DOM and experimental measurements. As can be seen from the figure, the incident flux decreases from the bed surface towards the cooler ones. The predictions are in good agreement with the MOL of DOM and the measurements [27].

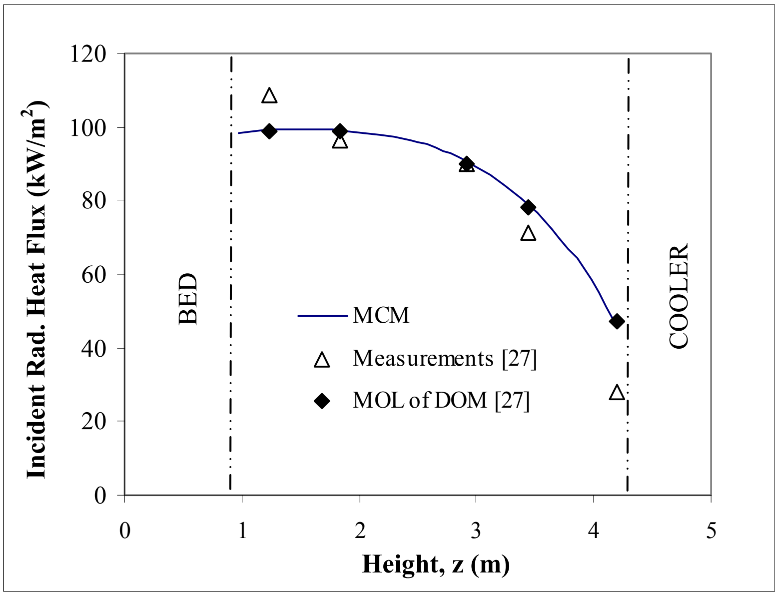

Fig. 6.9 Incident radiative heat fluxes on freeboard wall

A heat flux transducer is used to measure the incident radiative heat fluxes on the walls of the freeboard [27]. The measurements are taken during the steady-state operation of the ABFBC. The experimental measurements are given in detail in the references [26, 27, 28, and 29]. The predicted and measured values are a little different at the ports adjacent to the bed and cooler surfaces. Because, the cooling tubes at the bed and cooler surfaces affected the radiometer probe measurements adjacent to the top and bottom surfaces.

For comparative testing purposes, the values of the predicted fluxes are compared with the measurements at discrete points. Table 6.4 illustrates the relative percentage errors in the fluxes predicted by both methods. As can be seen from the table, percentage errors are very close to each other.

Table 6.4 Incident radiative heat fluxes on freeboard wall

		Predictions(kw/m^2)		Relative Error (%)	
Height (m)	Experimental (kw/m^2) [27]	MOL of DOM [27]	Monte Carlo*	MOL of DOM [27]	Monte Carlo*
1.23	108,9	99	98,9	-9,1	-9,0
1.83	96,4	98,8	99,5	2,5	3,0
2.91	90,2	90,1	90,9	-0,1	0,5
3.44	71,5	78	78,6	9,1	9,7
4.19	28	47,3	46,8	68,9	67,2

*1x1x25 subvolume is used in Monte Carlo Solution

* CPU time for Monte Carlo Solution is, 173.9 s for 4.2E6 total number of photon histories

6.2.3 Parametric studies

Sensitivity of the incident heat flux to the presence of particles is analyzed by comparing the predictions of MCM with and without particles (Fig. 6.10). As it can be seen from the figure, the effect of particles on the predicted heat fluxes is not considerable.

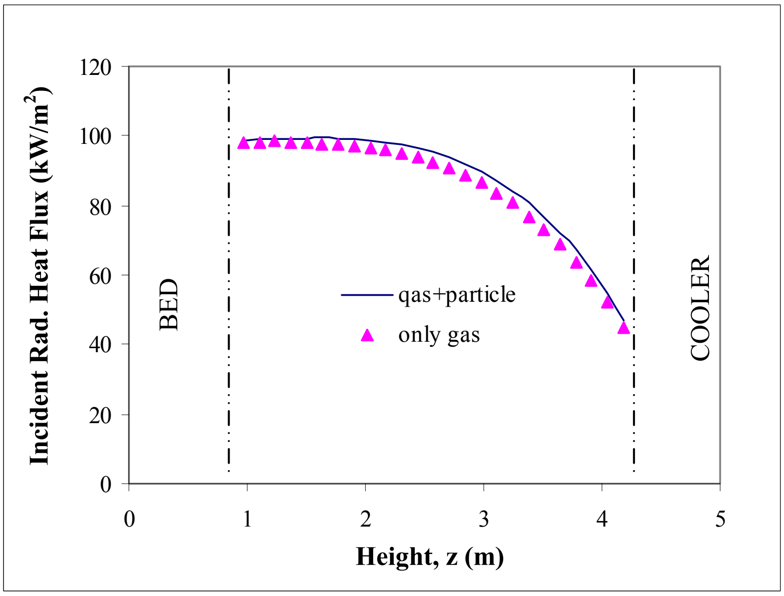

Fig. 6.10 Sensitivity of radiative heat flux to the presence of particles

CPU time for gas+particle and only gas cases are given at Table 6.5 below for 11E6 total number of photon histories used in the calculations.

The effects of particle load and anisotropic scattering on the incident heat fluxes are examined. The real case analyzed previously with isotropic scattering assumption is taken as the basis, and three different cases are generated by increasing the particle load and/or by incorporating strong anisotropy into the problem. The effect of anisotropy is analyzed by utilizing linear anisotropy assumption,

$$\Phi(\hat{s}\cdot\hat{s}') = 1 + A_1\hat{s}\cdot\hat{s}' = 1 + A_1 \cos\theta' \qquad (6.2)$$

where it is assumed that the polar angle θ' is measured from an axis pointing into the $\hat{s}$. A_1 is equal to 1 for the strong forward scattering case. In addition to the anisotropic case, a high particle load case is also investigated. The particle load is increased 1000 times which leads to, $\kappa \approx 160$ (absorption coefficient of the medium) and $\sigma_s \approx 450$ (scattering coefficient of the medium). CPU times are given in Table 6.5 for 220E6 total number of photon histories.

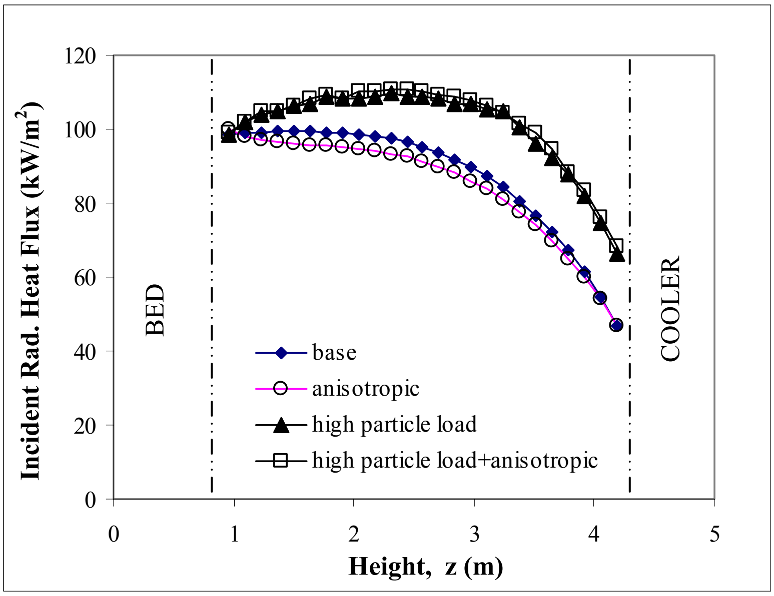

Fig.6.11 Effect of high particle load and anisotropy on incident radiative flux

Table 6.5 CPU times of parametric studies

	Gas + particle	Only gas	Base	Anisotropic	High particle load	High particle load + anisotropic
CPU Time, s	210.4	225.2	4504.7	4300.8	3199.9	2992.5

Finally, the net radiative heat flux at the freeboard walls is investigated. The main parameter investigated upto here is the incident radiative heat transfer. In most of the real engineering problems, net radiative heat transfer is a more important parameter. The net radiative heat flux is found by applying MCM to the freeboard problem. It can be concluded from Fig. 6.12 that the maximum net radiative heat flux occurs in the enclosure where the temperature difference between the wall and the medium is maximum. CPU time is 20139 s for 1.13E9 total number of photon histories.

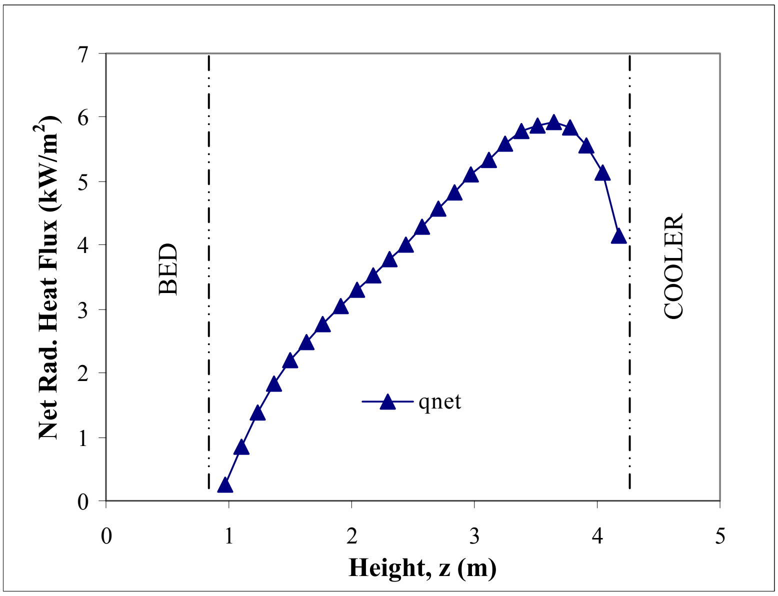

Fig.6.12 Net Radiative Heat Flux at the freeboard wall

CHAPTER 7

CONCLUSIONS AND FUTURE WORK

7.1 CONCLUSIONS

The accuracy of Monte Carlo method is re-examined by applying it to three-dimensional radiative heat transfer problems with participating media and comparing its predictions against measurements and/or benchmark solutions reported in the literature.

The predictive accuracy of the method is examined for:

- Cubical enclosure problems containing purely scattering and absorbing, emitting scattering media with isotropic and anisotropic scattering properties by validating the solutions against MOL of DOM solutions available in the literature,

and

- A physical problem, which is the freeboard of pilot-scale atmospheric, bubbling fluidized bed combustor by comparing its predictions with those of the MOL of DOM solutions and measurements.

The following conclusions have been reached on the basis of comparative testing procedure:

- MCM is predicting radiative heat transfer accurately in a cubical enclosure containing purely scattering medium. On the contrary, MCM results are oscillating through the MOL of DOM results for anisotropic cases. The grid spacing, and total number of photon emitted from the enclosure can be further investigated for anisotropic cases.

- When the results are considered, it could be concluded that the solution accuracy of the MCM is sufficient to predict radiative heat flux for three-dimensional problems with isotropically scattering media. The solutions of MCM for anisotropic media show some oscillation, but oscillations become smaller when sufficiently high numbers of total histories are used in the solution.

- MCM reproduces the measured incident radiative heat fluxes reasonably well for the freeboard problem.

- MCM is as accurate as the MOL of DOM.

Some parametric studies are also considered. Particle load effect and anisotropy on the predicted radiative fluxes are as follows,

- Presence of particles in the participating media does not affect the magnitude of predicted incident heat fluxes.

- Increasing the particle load an order of magnitude leads to significant rise in incident radiative fluxes at the wall.

Effect of anisotropy on the incident radiative heat fluxes on the side walls is negligible for the situation under consideration.

7.2 FUTURE WORK

Further developments can be utilized for the Monte Carlo method so that the problems at hand can be extended to involve nonhomogeneous and nongrey media.

The Monte Carlo method can efficiently be utilized in complete combustion models considering the increase in capability of computers and with the use of parallel processing.

REFERENCES

1. J.R. Howell and M. Perlmutter, 1964, "Monte Carlo Solution of Thermal Transfer Through Radiant Media Between Gray Walls", *Journal of Heat Transfer*, vol. 86 (1), pp. 116-122

2. C. M. Usiskin and E.M. Sparrow, 1960, "Thermal radiation between parallel plates separated by an absorbing-emitting-non-isothermal gas", *Intern. J. Heat and Mass Transfer* 1, 28

3. R. G. Deissler, 1964, "Diffusion approximation for thermal radiation in gases with jump boundary condition", *J. Heat Transfer* 86, 240

4. J.R. Howell and M. Perlmutter, 1964, "Radiant Transfer Through a Gray Gas Between Concentric Cylinders Using Monte Carlo", *Journal of Heat Transfer*, vol. 86 (2), pp. 169-179

5. J.R. Howell, 1968, "Application of Monte Carlo to Heat Transfer Problems", *Advances in Heat Transfer*, vol. 5, pp.1-55, Academic Press, New York

6. A. Hajii Sheikh, 1998, "Monte Carlo Methods", in: *Handbook of Numerical Heat Transfer* edited by W.J. Minkowycz et al, pp.673-723, Wiley, New York

7. A. Mochida, K. Kudo, Y. Mizutani, M. Hattori, Y. Nakamura, 1997, "Transient Heat Transfer Analysis in Vacuum Furnaces Heated By

Radiant Tube Burners", *Energy Convers. Mgmt*, vol.38 No10-13, pp.1169-1176

8. H. Taniguchi, O. Toshiaki, M. Iwata, N. Arai, K. Hiraga, S. Yamaguchi, 2002, "Numerical Study of Radiation-Convection Heat Transfer", *Heat Transfer-Asian Research*, vol. 31(5), pp. 391-407

9. L. H. Liu, H. P. Tan, Q. Z. Yu, 2003, "Temperature Distributions in an Absorbing–Emitting–Scattering Semitransparent Slab with Variable Spatial Refractive Index", *International Journal of Heat and Mass Transfer*, pp.2917-2920

10. P.B. Abdallah, V. Le Dez, 2000, "Thermal field inside an absorbing, emitting, semi-transparent slab at radiative equilibrium with variable spatial refractive index", *J. Quant. Spectrosc. Radiat. Transfer*, vol 65, pp. 595–608

11. L. H. Liu, X. Xu, 2003, "Monte Carlo Ray-Tracing simulation for Radiative Heat Transfer in Turbulent Fluctuation Media under the Optically Thin Fluctuation Approximation", *Journal of Quantitative Spectroscopy and Radiative Transfer*, pp. 1-7

12. R. Vaillon, B.T. Wong, P. Mengüç, 2003, " Polarized Radiative Transfer in a Particle-laden Semi-transparent Medium via a Vector Monte Carlo Method", *Proceedings of Eurotherm 73 on Computational Thermal Radiation in Participating Media*

13. R. Couqard, D. Baillis, D. Quenard, 2003, "Radiative Properties of Semi-transparent Spherical Particle Beds, *Proceedings of Eurotherm 73 on Computational Thermal Radiation in Participating Media*

14. A. Snergiev, 2003, “ Monte Carlo Modelling of Radiative Transfer in Unconfined Buoyant Turbulent Diffusion Flames”, *Proceedings of Eurotherm 73 on Computational Thermal Radiation in Participating Media*

15. B.T. Wong, P. Mengüç, 2003, “Monte Carlo Methods in Radiative Transfer and Electron-beam Processing”, *Proceedings of Eurotherm 73 on Computational Thermal Radiation in Participating Media*

16. Q. Yu, L. Liu, Y. Pan, D. Zhang, J. Ji, and H. Ta, 1999, “Monte Carlo Method for Simulating the Radiative Characteristic of an Anisotropic Medium”, *Journal of Heat Transfer Asian Research*, vol. 28 (3), pp. 201-210

17. J.G.Marakis, C.Papapavlou, E.Kakara, 2000, “A parametric Study of Radiative Heat Transfer in Pulverised Coal Furnace”, *International Journal of Heat and MassTransfer*, vol. 43, pp. 2961-2971

18. W. Chai, 1997, “Radiative Heat Transfer Model in Arbitrary Enclosures by Ray-Tracing”, *Proceedings of the 2nd International Symposium on Radiation Transfer*, edited by P. Mengüç, Begell House, New York, pp. 55-73

19. H. Ertürk, F. Arınç, N. Selçuk, 1997, “Accuracy of Monte Carlo Method Re-examined on a Box-shaped Furnace Problem”, *Proceedings of the 2nd International Symposium on Radiation Transfer*, edited by P. Mengüç, Begell House, New York, pp. 85-95

20. H. Ertürk, 1997, “Mathematical Modeling of Radiative Heat Transfer in Participating Meida”, Metu, *Msc. Thesis*

21. N. Selçuk, 1981, “Fırınlardaki Işınım Isı Transferinin Tam Çözümü ve Akı Yöntemlerinin İrdelenmesi”, ODTÜ, *Doçentlik Tezi*

22. N. Selçuk, 1985, “Exact Solutions for Radiative Heat Transfer in Box-Shaped Furnaces”, *ASME Journal of Heat Transfer*, vol. 107, pp.648-655

23. T.W. Tong and R.D. Skocypec, 1992, “Summary on Comparison of Radiative Heat Transfer Solutions for a Specified Problem”, *ASME HTD-Developments in Radiative Heat Transfer*, Vol. 203, pp.253-258

24. I. Ayrancı, 2001, “The Method of Lines Solution of Discrete Ordinates Method for Radiative Heat Transfer in 3-D Rectangular Enclosures Containing Scattering Media”, Metu, *Msc. Thesis*

25. S. H. Kim, K. Y. Huh, 2000, “A new Angular Discretization Scheme of the Finite Volume Method for 3-D Radiative Heat Transfer in Absorbing, Emitting and Anisotropically Scattering Media”, *Int. J. Heat Mass Transfer*, Vol. 43, pp. 1233-1242

26. A. Batu, N. Selçuk, 2002, “Modeling of Radiative Heat Transfer in the Freeboard of a Fluidized Bed Combustor Using the Zone Method of Analysis”, *Turkish J. Eng. Env. Sci.*, vol.26, pp. 49-58

27. N. Selçuk, A. Batu, I. Ayrancı, 2001, “Performance of Method of Lines Solution of Discrete Ordinates Method in the Freeboard of a Bubbling Fludized Bed Combustor”, *Proceedings of the 3rd International Symposium on Radiation Transfer*, edited by P. Mengüç and N. Selçuk, Begell House, New York, pp. 527-538

28. M. Kozan, 1999, “Investigation of Radiative Heat Transfer in Freeboard of a 0.3 MWt AFBC Test Rig”, METU, *Msc. Thesis*

29. M. Kozan, N. Selçuk, 2000, “Investigation of Radiative Heat Transfer in Freeboard of a 0.3 MWt AFBC Test Rig”, *Combust. Sci. Tech. Vol*. 153, pp 113-126

30. M.F. Modest, 1993, *Radiative Heat Transfer*, McGraw Hill, New York

31. T.-K. Kim and H Lee, 1988, “Effect of Anisotropic Scattering on Radiative Heat Transfer in Two-dimensional Rectangular Enclosures”, *Int. J. of Heat Transfer*, Vol.31(8), pp.1711-1721

32. N. Selçuk, E. Değirmenci and Y. Göğebakan, 2000, “Assessment of Catalyst Deactivation Model for Sulfur Rtention in Fluidized Bed Combustors”, *Combust. Sci. Tech*., Vol. 153, pp 95-111

33. E. Değirmenci, 2000, “Dynamic Simulation of Fludized Bed Combustors”, METU, *PhD. Thesis*

34. R. Siegel and J.R. Howell, 1992, “Thermal Radiation Heat Transfer”, 3rd ed., *Hemisphere*, Washington

35. F.P. Incropera, and D.P. DeWitt, 1994, “Fundamentals of Heat and Mass Transfer”, 4th ed., *John Wiley and Sons*, New York

APPENDIX A

FLOW CHARTS

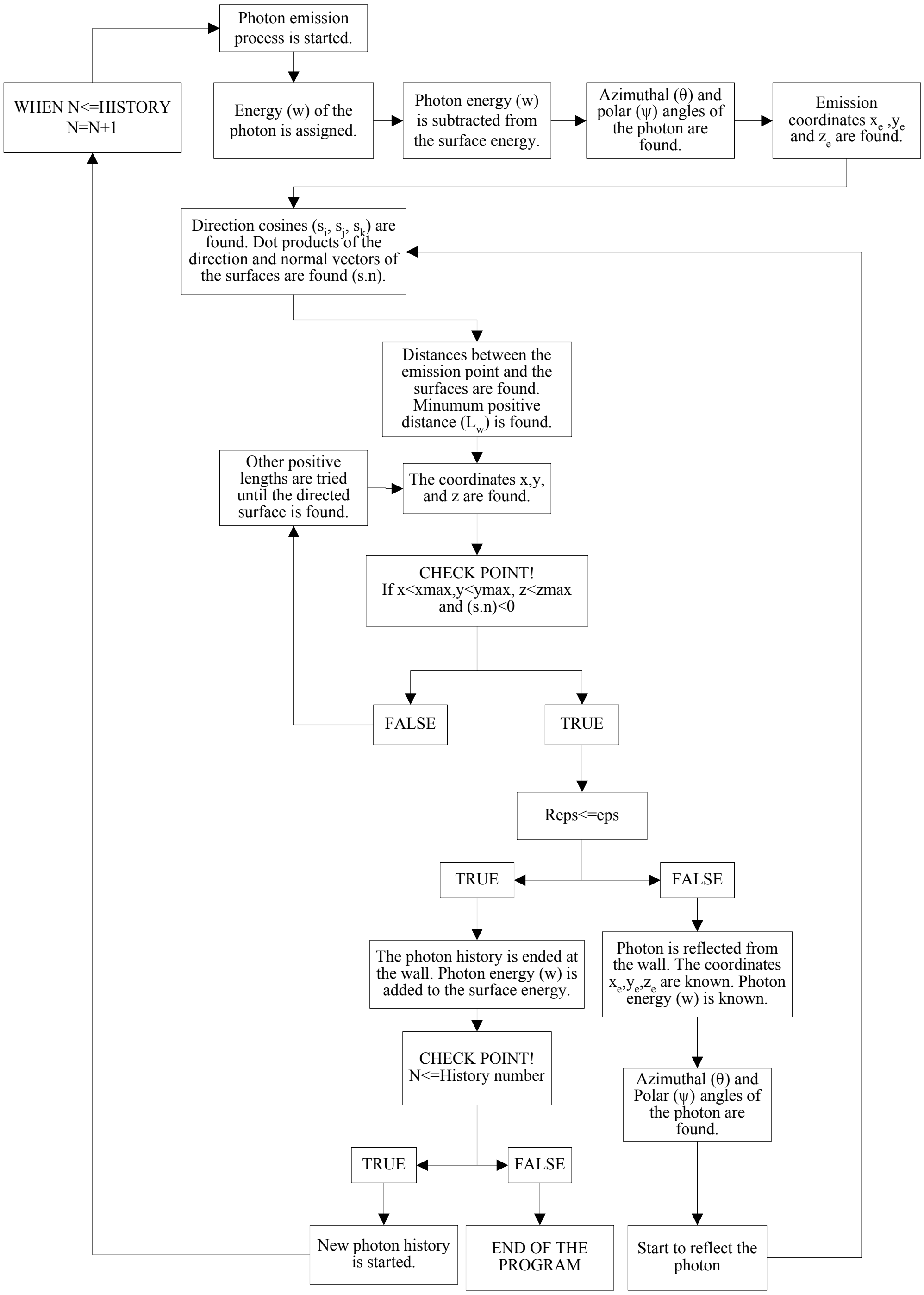

Figure A.1 Flow Chart for non-participating medium problems.

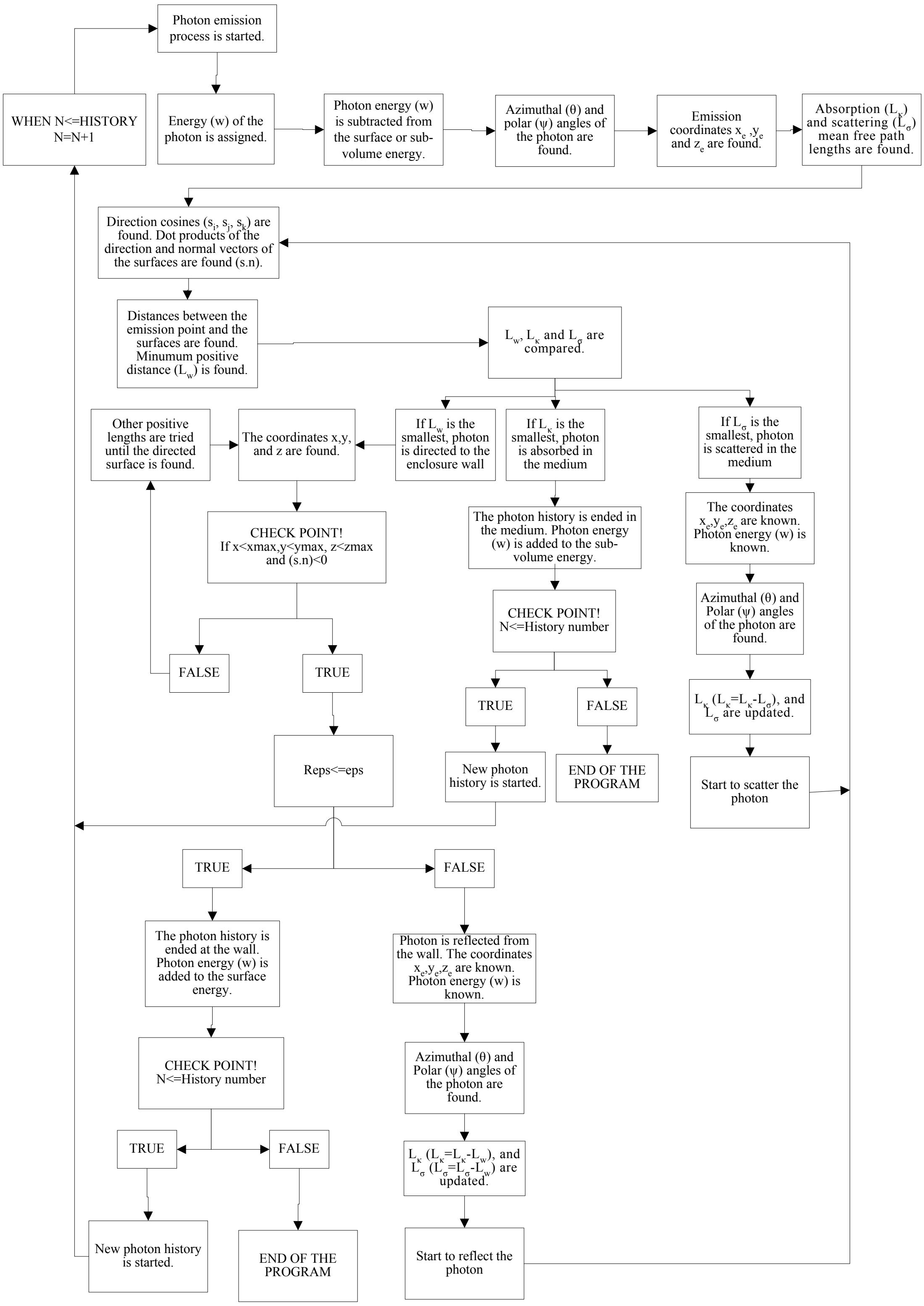

Figure A.2 Flow Chart for cubical enclosure problems

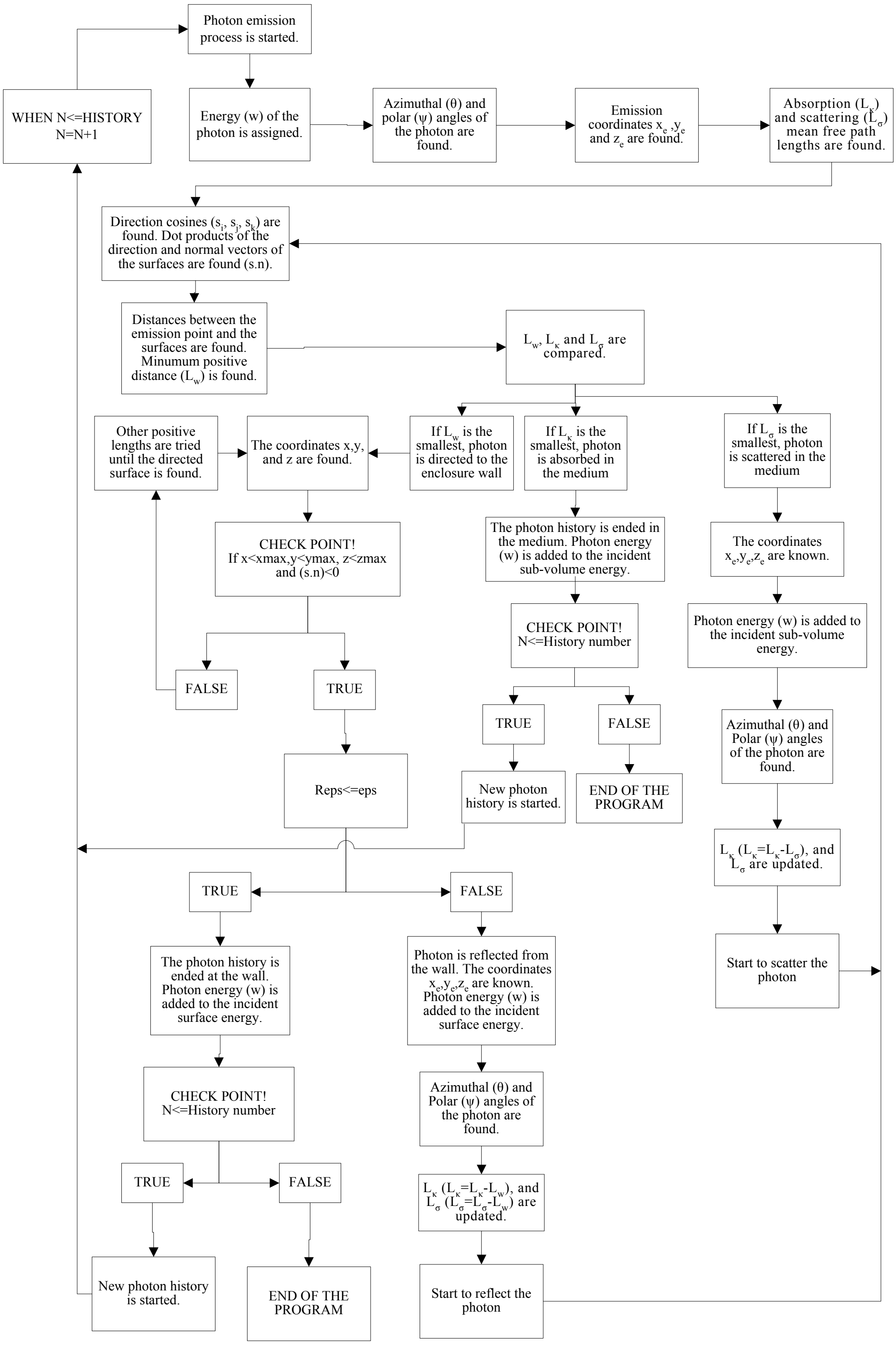

Figure A.3 Flow Chart for freeboard problems